



Metabolic division engineering of *Escherichia coli* consortia for *de novo* biosynthesis of flavonoids and flavonoid glycosides

Zetian Qiu^{a,b,d}, Yumei Han^{a,c,d}, Jia Li^{a,d}, Yi Ren^{a,d}, Xue Liu^{a,d},
Shengying Li^{b,e,*}, Guang-Rong Zhao^{a,d,**}, Lei Du^{b,***}

^a State Key Laboratory of Synthetic Biology, School of Chemical Engineering and Technology, Tianjin University, Yaguan Road 135, Jinnan District, Tianjin, 300350, China

^b State Key Laboratory of Microbial Technology, Shandong University, Qingdao, Shandong, 266237, China

^c College of Life Science and Technology, Huazhong Agricultural University, Wuhan, 430070, China

^d Georgia Tech Shenzhen Institute, Tianjin University, Dashi Road 1, Nanshan District, Shenzhen, 518055, China

^e Laboratory for Marine Biology and Biotechnology, Qingdao Marine Science and Technology Center, Qingdao, Shandong, 266237, China

ARTICLE INFO

Keywords:

Flavonoids
Flavonoid glycosides
Synthetic biology
Metabolic engineering
Metabolic division engineering
Coculture

ABSTRACT

Heterologous biosynthesis of natural products with long biosynthetic pathways in microorganisms often suffers from diverse problems, such as enzyme promiscuity and metabolic burden. Flavonoids and their glycosides are important phytochemicals in the diet of human beings, with various health benefits and biological activities. Despite previous efforts and achievements, efficient microbial production of plant-derived flavonoid compounds with long pathways remains challenging. Herein, we applied metabolic division engineering of *Escherichia coli* consortia to overcome these limitations. By establishing new biosynthetic pathways, rationally adjusting metabolic node intermediates, and engineering different auxotrophic and orthogonal carbon sources for hosts, we established stable two- and three-bacteria co-culture systems to efficiently *de novo* produce 12 flavonoids (61.15–325.31 mg/L) and 36 corresponding flavonoid glycosides (1.31–191.79 mg/L). Furthermore, the co-culture system was rapidly extended in a plug-and-play manner to produce isoflavonoids, dihydrochalcones, and their glycosides. This study successfully alleviates metabolic burden and overcomes enzyme promiscuity, and provides significant insights that could guide the biosynthesis of other complex secondary metabolites.

1. Introduction

Heterologous biosynthesis of natural products frequently encounters great challenges, including enzyme promiscuity and metabolic burden, particularly in those with long biosynthetic pathways (Cheah et al., 2023; Chen et al., 2019; Sun et al., 2022). The promiscuity in enzyme activity often leads to the generation of by-products and seriously decreases the efficiency of the intricate biosynthetic routes (Brooks et al., 2023; Liu et al., 2024; Qiu et al., 2022). The introduction and over-expression of a lengthy biosynthetic pathway would intensify the metabolic burden on the host organism, adversely affecting both cell growth and the product yield (Yang et al., 2024). In some plants, metabolic efficiency can be optimized by minimizing enzyme

promiscuity through enabling specific protein-protein interactions between metabolic enzymes and endogenous proteins (Waki et al., 2021). However, overcoming these problems in heterologous microbial systems remains challenging, which restricts the bioproduction of many valuable bioactive compounds.

Flavonoids, one of the largest families of natural products, are mainly diverse groups of plant-derived polyphenols, with approximately 10,000 known structures to date (Lv et al., 2019). Many of the flavonoids (e.g., taxifolin) exhibit various biological activities and health benefits, and are widely applied in food, pharmaceutical, nutraceutical, and cosmetic industries (Jucá et al., 2020; Xiong et al., 2016). Flavonoids can exist as aglycone and glycoside forms, with the latter (e.g., diosmin) possessing improved properties such as stability, solubility, and bioavailability

* Corresponding author. State Key Laboratory of Microbial Technology, Shandong University, Qingdao, Shandong, 266237, China.

** Corresponding author. State Key Laboratory of Synthetic Biology, School of Chemical Engineering and Technology, Tianjin University, Yaguan Road 135, Jinnan District, Tianjin, 300350, China.

*** Corresponding author.

E-mail addresses: lishengying@sdu.edu.cn (S. Li), grzhao@tju.edu.cn (G.-R. Zhao), lei.du@sdu.edu.cn (L. Du).

<https://doi.org/10.1016/j.ymben.2025.02.001>

Received 26 November 2024; Received in revised form 17 January 2025; Accepted 9 February 2025

Available online 11 February 2025

1096-7176/© 2025 International Metabolic Engineering Society. Published by Elsevier Inc. All rights are reserved, including those for text and data mining, AI training, and similar technologies.

(Hofer, 2016; Ji et al., 2020). The sugar moieties in flavonoid glycosides greatly influence their physiological effects and applications (Duan et al., 2023; Wang et al., 2024b). Some flavonoid glycosides have been commercialized as drugs or health products for treating different disorders (Gerges et al., 2022). The global market for flavonoids and their derivatives is projected to reach 1.5 billion USD by 2025, creating a high

demand for large-scale production (Bennett et al., 2021).

However, the natural abundance of flavonoids and their glycosylated forms is often limited, making extraction difficult and costly (Chaves et al., 2020). Biotransformation provides an environmentally friendly alternative for synthesizing these molecules under mild conditions (Lan et al., 2023). Nevertheless, the long biosynthetic pathways for

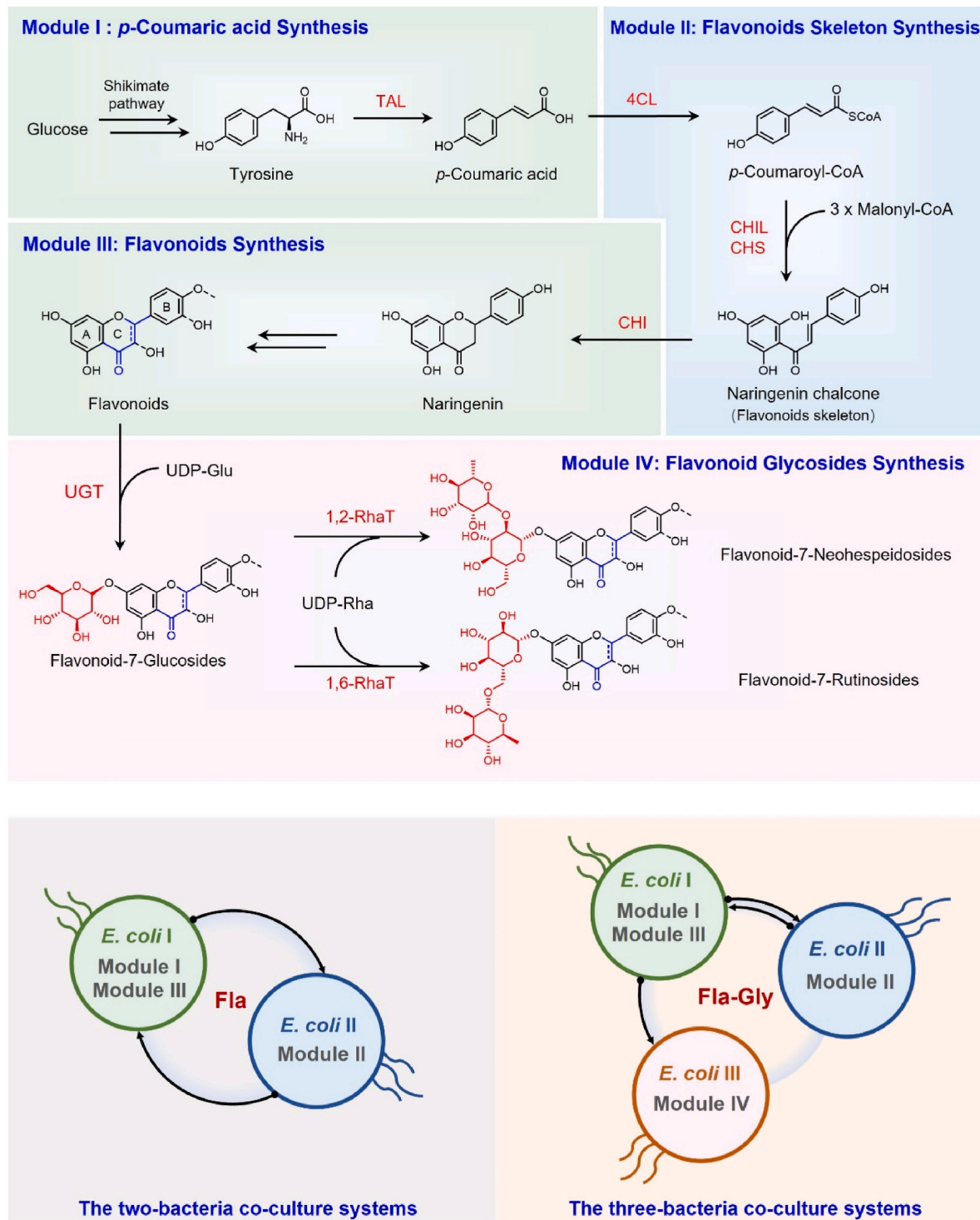


Fig. 1. *De novo* production of flavonoids and flavonoid glycosides by metabolic division engineering of *E. coli* consortia. Upper panel, the biosynthetic pathway of flavonoids and flavonoid glycosides. Lower panel, the two-bacteria co-culture systems for synthesizing flavonoids and the three-bacteria co-culture systems for synthesizing flavonoid glycosides. TAL: tyrosine ammonia lyase; 4CL: 4-coumarate-CoA ligase; CHS: chalcone synthase; CHIL: chalcone isomerase-like protein; CHI: chalcone isomerase; UGT: UDP-glucuronosyltransferase; 1,2-RhaT: 1,2-rhamnosyltransferase; 1,6-RhaT: 1,6-rhamnosyltransferase; UDP-Glu: UDP-glucose; UDP-Rha: UDP-rhamnose; Fla: flavonoids; Fla-Gly: flavonoid-7-glycosides.

flavonoids and flavonoid glycosides impose a metabolic burden on the host cells, and the enzyme promiscuity often results in the formation of branched pathways and unwanted by-products (Falcone Ferreyra et al., 2012). The transmembrane mechanism of flavonoids in microorganisms remains incompletely understood. However, their lipid-soluble nature suggests that flavonoids may traverse the cell membrane through passive diffusion (Kiryama et al., 2024). Modular coculture, an emerging technique for flavonoid biosynthesis, frequently utilizes *Escherichia coli* due to its rapid growth, low nutrient needs, and well-developed tools for genetic engineering (Liu et al., 2023). Some *E. coli* co-culture systems have been established to *de novo* produce flavonoids and other bioactive natural products such as silibinin, rosmarinic acid, and sclareolide (Pan et al., 2023; Tang et al., 2024; Wang et al., 2023a). However, the low yield and high cost of flavonoids and glycosylated forms are prohibitive for large scale production. According to previous reports, three major bottlenecks restrict the efficiency of flavonoids and flavonoid glycosides production: (1) short of natural metabolic pathways and alternative enzymes; (2) rate-limiting steps in the biosynthetic pathway causing precursor limitation; and (3) suboptimal selection of intercellular node compounds and allocation of metabolic modules leading to poor coordination of metabolic flux, severe side reactions, and unnecessary by-products. Therefore, it is crucial to overcome these challenges to design and construct more effective microbial systems for synthesizing flavonoids and their glycosides.

In this study, we developed two- and three-strain *E. coli* consortia through metabolic division engineering strategy for the efficient *de novo* biosynthesis of various flavonoids and glycosides, respectively. We decoupled and distributed the synthesis of different metabolites, developing specialized *E. coli* strains with distinct synthetic modules responsible for the biosynthesis of *p*-coumaric acid, construction of the flavonoid skeleton, assembly of flavonoid structures, and synthesis of flavonoid glycosides (Fig. 1). We optimized the selection of node compounds in different modules and reduced by-products through metabolic allocation engineering, achieving unprecedented yield in the *de novo* synthesis of a range of flavonoids and their glycosides, including the first synthesis of various flavonoid-7-diglycosides. Furthermore, we employed obligate mutualistic engineering of multi-metabolite cross-feeding to significantly stabilize co-culture systems. Using strategies such as module replacement and plug-and-play, our systematically designed co-culture systems successfully synthesized other non-traditional flavonoids and glycosides, thereof including isoflavonoids (with B ring connected at the 3-position of the C ring) and dihydrochalcones (lacking the C ring) (Supplementary Fig. S1). We anticipate that metabolic division engineering of microbial consortia be a promising strategy for large-scale and sustainable production of other complex compounds.

2. Materials and methods

2.1. Media and chemicals

Strains for gene cloning, plasmid propagation, and inoculum preparation were cultured in Luria–Bertani (LB) medium composed of 5.00 g/L yeast extract, 10.00 g/L tryptone, and 10.00 g/L NaCl. Batch fermentations were performed using M9 basic medium, comprising 6.78 g/L Na₂HPO₄, 3.00 g/L KH₂PO₄, 1.00 g/L NH₄Cl, 0.50 g/L NaCl, 120.00 mg/L MgSO₄, 11.00 mg/L CaCl₂ and 1.00 mL/L trace element solution. The trace element solution included 0.03 mg/L H₃BO₃, 0.38 mg/L CuCl₂, 0.40 mg/L Na₂EDTA, 0.50 mg/L CoCl₂, 0.94 mg/L ZnCl₂, 1.60 mg/L MnCl₂, 3.60 mg/L FeCl₂, and 100.00 mg/L Thiamine. M9Y medium (M9 minimal medium supplemented with 1.00 g/L yeast extract) was used for single strains *de novo* synthesized *p*-coumaric acid and whole-cell catalytic synthesis of flavonoids or flavonoid glycosides. M9A medium (M9 basic medium supplemented with 50.00 mg/L of necessary amino acids) was used for obligate mutualistic co-culture system fermentation. For strains lacking the *Dahms* pathway and decouple

glycolysis and the tricarboxylic acid cycle, carboxylic acids (2.00 g/L of sodium pyruvate, 2.00 g/L of malic acid, 2.00 g/L of succinic acid, and 2.00 g/L of oxaloacetic acid) were added to the culture medium. As needed, carbon sources such as glucose, xylose, arabinose, propane-1,2,3-triol, sucrose, dextrin, and cellobiose were added to the culture medium at a final concentration of 10.00 g/L. Appropriate antibiotics (30.00 mg/L kanamycin, 50.00 mg/L ampicillin, 30.00 mg/L streptomycin, and 30.00 mg/L chloramphenicol) were added to the culture medium. All flavonoids and flavonoid-glycosides used in this study were commercially available and were obtained from Heowns Biotech (Tianjin, China), Dingguo Biotech (Tianjin, China), Guangao Biotech (Wuhan, China), Herbsubstance Biotech (Chengdu, China), or Yuanye Biotech (Shanghai, China).

2.2. Plasmids and strains construction

The source and accession number of enzymes in this study are listed in Supplementary Table S1. The strains and plasmids used in this study are listed in Supplementary Table S2. The primers in this study for gene amplification or plasmid construction were synthesized by Sangon Biotech (Shanghai, China) and are listed in Supplementary Table S9. Plasmids pET28b (ultra-high copy), pETduet1 (high copy), pCDFduet1 (medium copy), and pACYCduet1 (low copy) were used for pathway assembly. Codon-optimized heterologous gene fragments were synthesized by BGI Genomics (Shenzhen, China). Phanta Max Super-Fidelity DNA Polymerase (Vazyme Biotech, Nanjing, China) was used for polymerase chain reaction. Universal DNA Purification Kit (Tiangen Biotech, Beijing, China) was used for DNA fragment purification. In vitro recombination was performed to construct plasmids using ClonExpress Ultra One Step Cloning Kit (Vazyme Biotech, Nanjing, China). HighPure Maxi Plasmid Kit (Tiangen Biotech, Beijing, China) was used for plasmid isolation. Target gene was amplified using the corresponding primers in Supplementary Table S9, and cloned into the linearized vectors.

Gene knockout and chromosomal integration were performed using CRISPR-Cas9-mediated RED recombination following standard protocols. Plasmids used for gene knockout and chromosomal integration are listed in Supplementary Table S3. Plasmid pCas was introduced into the host cell. The strain carrying pCas was cultured in LB medium containing 10.00 g/L arabinose and prepared as competent cells. Overlap PCR and multi-fragment homologous recombination were used to construct a helper plasmid containing the upstream and downstream homology arm fragments of the target site, gRNA fragment, and inserted gene cassette. The helper plasmid was introduced into the pCas-carrying strain and spread on LB agar plates containing 50.00 mg/L kanamycin and 100.00 mg/L tetracycline. Deletion of target genes and integration of heterologous genes were confirmed by colony direct PCR.

2.3. Shake flask fermentation

The engineered *E. coli* strains were cultured in 3 mL of LB medium overnight at 37 °C and 220 rpm, followed by inoculation into 50 mL of LB medium at a ratio of 1:100. When cell density of OD₆₀₀ reaches 0.8–1.2, the cells were collected by centrifugation, washed twice with sterile water, and inoculated into the fermentation medium. 0.2 mM isopropyl β-d-1-thiogalactopyranoside (IPTG) and 200.00 mg/L substrate were added at OD₆₀₀ of 0.5. Sodium malonate (2.00 g/L) was added into the medium of the strain with malonate assimilation pathway. The *E. coli* strains in the coculture system were inoculated based on the specified initial inoculation ratio, maintaining a total initial OD₆₀₀ of 1.0 and IPTG of 0.2 mM. During the 48 h fermentation process, conducted at 30 °C with shaking at 220 rpm, samples were periodically collected to determine both the biomass at OD₆₀₀ and metabolite concentrations. In co-culture systems, subpopulation ratios were analyzed.

2.4. Extraction and analysis of fermentation broth

Fermentation broth samples were collected and washed three times with sterile water. The biomass at OD₆₀₀ was measured using a TU-1810 spectrophotometer. Following centrifugation and filtration of the fermentation broth with a 0.22 μm filter, the supernatant was determined at 340 nm on the same spectrophotometer to assess the relative content of red flaviolin. An equal volume of ethyl acetate and 0.05 g quartz sand were added to the fermentation broth, followed by vortexing for 1 h, centrifugation at 7500 rpm for 5 min. And then the organic layer was collected. Subsequently, the organic phase was evaporated dryness under nitrogen, and the resultant solute was dissolved in 1 mL of methanol. Flavonoid metabolites were analyzed using an Agilent 1260 system equipped with a photodiode array detector and a Hypersil™ BDS C18 column (150 × 4.6 mm, 5 μm particle size, Thermo Fisher Scientific, US). The mobile phase consisted of a 60:40 mixture of solvent A (0.1% formic acid in water) and solvent C (0.1% formic acid in methanol).

Isocratic separation was carried out over 35 min at the flow rate of 1 mL/min, with the column temperature maintained at 35 °C. The fermentation broth for flavonoid glycoside biosynthesis was mixed with an equal volume of methanol, vortexed for 1 h, centrifuged at 7500 rpm for 5 min, and filtered through a 0.22 μm filter. The supernatant was then subjected to analysis using an Agilent 1260 system equipped with a

photodiode array detector and a Hypersil™ BDS column (250 × 4.6 mm, 5 μm particle size, Thermo Fisher Scientific, US). The mobile phase consisted of water (solvent A) and acetonitrile (solvent B) with 0.1% trifluoroacetic acid (TFA). A linear gradient elution was applied with the following specific time intervals and buffer percentages: 5–10% solvent B (10–15 min); 10–20% solvent B (15–20 min); 20–33% solvent B (20–43 min); 33–60 % solvent B (43–45 min); 60% solvent B (45–47 min); 60-5% solvent B (47–50 min); 5% solvent B (50–57 min). The sample was separated for 57 min at a flow rate of 0.8 mL/min and a column temperature of 30 °C. High-resolution MS analysis of flavones and flavonoid glycosides was conducted in negative ion mode with a Synapt G2-Si Q-TOF mass spectrometer and an ACQUITY UPLC system from Waters.

2.5. Subpopulation analysis of coculture systems

In the two-bacteria co-culture system for flavonoid synthesis, one strain was engineered to express the blue fluorescent protein gene (*mElectra1*), while the other expressed the red fluorescent protein gene (*Tdtomato*). After sampling, the strains were washed with phosphate-buffered saline, diluted appropriately, and plated on the appropriate resistance LB agar plates, followed by overnight incubation at 37 °C. The colonies were illuminated with 480 nm excitation light source. The cell

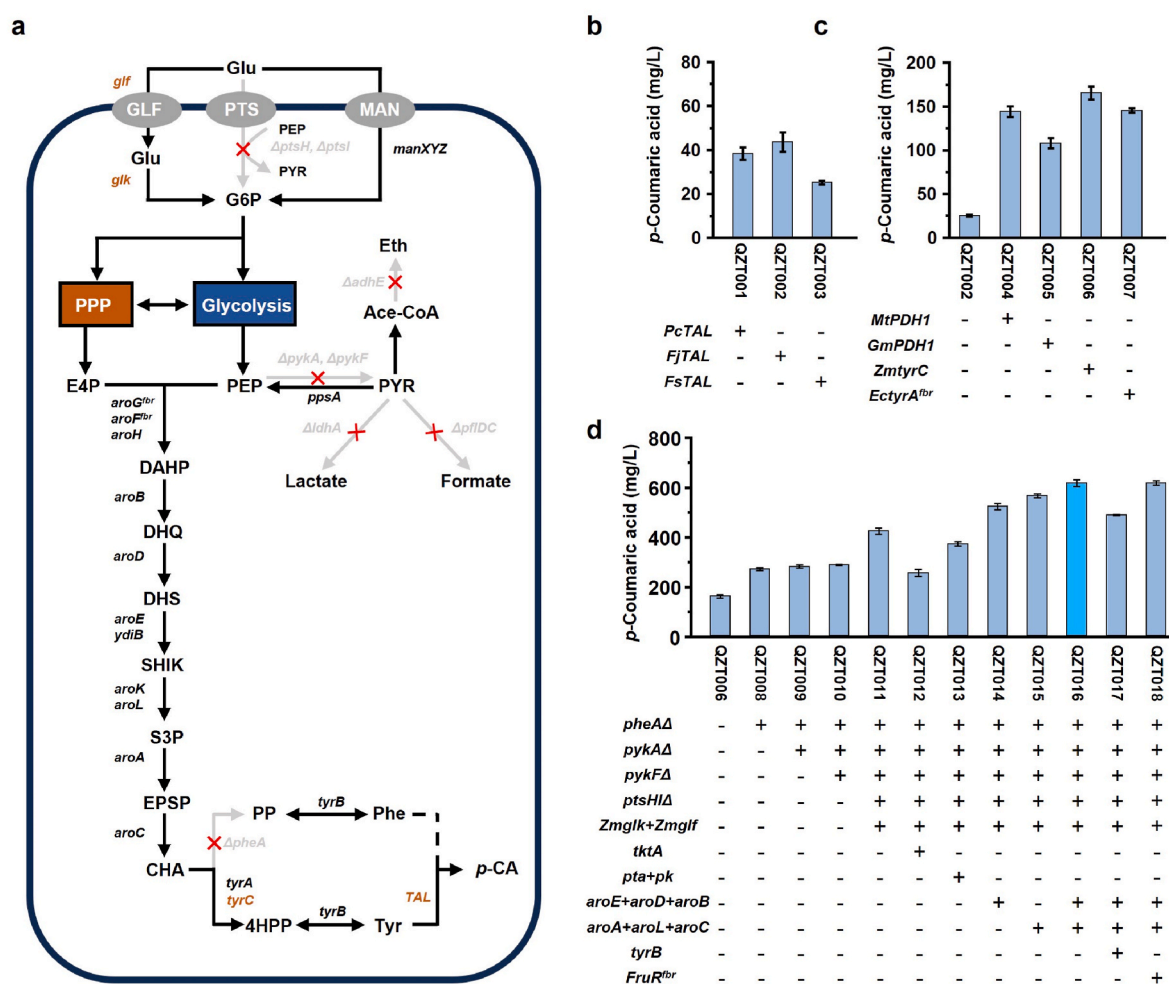


Fig. 2. Construction of *E. coli* for the synthesis of *p*-coumaric acid. (a) Biosynthetic pathway of *p*-coumaric acid. (b) Production of *p*-coumaric acid in QZT001 to QZT003 expressing different TALs. (c) Production of *p*-coumaric acid expressing different tyrosine prephenate dehydrogenases. (d) Production of *p*-coumaric acid remodeling *E. coli* cells. Data shown are mean ± SD (n = 3 independent experiments). Glu: glucose; G6P: glucose 6-phosphate; PPP: pentose phosphate pathway; E4P: erythrose-4-phosphate; PEP: phosphoenolpyruvate; PYR: pyruvate; DAHP: 3-deoxy-D-arabinoheptulosonate 7-phosphate; DHQ: 3-dehydroquinic acid; DHS: dehydroshikimate; SHIK: shikimate; S3P: shikimate 3-phosphate; EPSP: 5-enolpyruvoylshikimate 3-phosphate; CHA: chorismic acid; PP: phenylpyruvate; 4HPP: 4-hydroxyphenylpyruvate; PHE: Phenylalanine; TYR: tyrosine; Eth: ethanol; Ace-CoA: acetyl-CoA.

ratios were determined by counting the blue and red colonies. In the three-bacteria co-culture system for flavonoid glycoside production, the genome of the flavonoid glycoside-synthesizing strain didn't carry fluorescent protein gene, while the other two strains expressed *mElectra1* and *TdTomato*, respectively. Following sample collection, the strains were cleansed with phosphate-buffered saline, adequately diluted, and then plated on LB agar with corresponding resistance. The population proportion of flavonoid glycoside-producing strains was quantitatively determined by counting the non-fluorescent colonies under 480 nm excitation. The proportions of the other two strains were determined by counting red and blue fluorescent colonies described above.

3. Results and discussion

3.1. Engineering *E. coli* for enhanced production of *p*-coumaric acid

Flavonoid-related compounds require *p*-coumaric acid as a key precursor, which is biosynthesized from phenylalanine or tyrosine through the shikimate pathway (Fig. 2a). To achieve high concentrations of *p*-coumaric acid, we employed *E. coli* NST74(DE3) (Sekar et al., 2019) as our original host, which relieved some of the feedback inhibition in the aromatic amino acid synthesis pathway (*aroF394fbr*, *pheA101fbr* and *aroG397fbr*). *p*-Coumaric acid can be synthesized from tyrosine through the catalysis of tyrosine ammonia lyase (TAL) or from phenylalanine through the cascade catalysis of cytochrome P450 (cinnamic acid 4-hydroxylase, C4H) and phenylalanine ammonia lyase (PAL). Considering the expression challenging of cytochrome P450 (cinnamate-4-hydroxylase, C4H) in *E. coli*, we chose tyrosine instead of phenylalanine as the precursor and evaluated three different sources of tyrosine ammonia lyase (TAL). The strain QZT002, which harbored *FjTAL* from *Flavobacterium johnsoniae*, proved to be optimal, producing 43.84 mg/L *p*-coumaric acid (Fig. 2b). To eliminate the feedback inhibition of *L*-tyrosine, we cloned and expressed three heterologous tyrosine prephenate dehydrogenase coding genes (*GmPDH1* from *Glycine max* (Schenck et al., 2017), *MtPDH1* from *Medicago truncatula* (Liu et al., 2019), and *ZmtyrC* from *Zymomonas mobilis* (Wang et al., 2023b)) and the endogenous feedback-resistant mutant *tyrA^{fbr}* gene (Qiu et al., 2022) in *E. coli*. These approaches effectively increased *p*-coumaric acid production, with *ZmtyrC* yielding the highest amount at 165.80 mg/L (Fig. 2c).

To further enhance *p*-coumaric acid synthesis, the *pheA* gene (coding phenylalanine prephenate dehydratase) was knocked out to prevent pathway diversion toward phenylalanine (Aulakh et al., 2023; Liu et al., 2018; Yao et al., 2013) (Fig. 2d, strain QZT008). The shikimate pathway is catalyzed by the condensation of two precursors: phosphoenolpyruvate (PEP) and erythrose-4-phosphate (E4P). To accumulate more PEP, the *pykA* and *pykF* genes (coding pyruvate kinase isoenzymes) were knocked out to block the metabolic flux associated with the conversion of PEP to pyruvate. Simultaneously, the phosphotransferase system (PTS system, including the *ptsH* and *ptsI* genes) was replaced with the *glf* and *glk* genes from *Zymomonas mobilis* (Chen et al., 2021) to avoid PEP consumption during glucose uptake. The resulting strain, QZT011, generated 438.76 mg/L *p*-coumaric acid in shake flask culture (Fig. 2d), reflecting an approximate 1.6-fold increase than strain QZT006 in production. E4P, derived from the pentose phosphate pathway (PPP), is another vital metabolite for cell growth. Various metabolic engineering strategies have been reported to enhance E4P biosynthesis, with the overexpression of transketolase *tktA* gene being identified as a key method (Koma et al., 2020). The incorporation of a heterologous phosphoketolase (PHK) pathway (including the *pta* and *pk* genes) can degrade fructose 6-phosphate (F6P) into acetyl phosphate and E4P, thereby optimizing E4P availability for aromatic biosynthesis (Liu et al., 2019). However, none of the aforementioned strategies for the E4P enhancement succeeded in increasing *p*-coumaric acid titers in our experiments (Fig. 2d, strain QZT012 and QZT013), although they have been previously reported to increase aromatic amino acid production.

We further strengthened the shikimate pathway by overexpressing upstream *aroE* (coding shikimate dehydrogenase), *aroD* (coding 3-dehydroquinate dehydratase) and *aroB* (coding 3-dehydroquinate synthase) genes and downstream *aroA* (coding 3-phosphoshikimate 1-carboxyvinyltransferase), *aroL* (coding shikimate kinase), *aroC* (coding 3-dehydroquinate synthase) genes. The strain overexpressing *aroE*, *aroD* and *aroB* produced 542.04 mg/L *p*-coumaric acid (Fig. 2d, strain QZT014), while *aroA*, *aroL* and *aroC* overexpression yielded 586.92 mg/L (strain QZT015). The highest yield of 640.25 mg/L (strain QZT016) was achieved by overexpressing *aroE*, *aroD*, *aroB*, *aroA*, *aroL* and *aroC* simultaneously. Interestingly, further overexpression of *tyrB* gene (coding tyrosine aminotransferase, involving in the final step of tyrosine biosynthesis) resulted in reduced *p*-coumaric acid production (strain QZT017). This may be because it can reversibly catalyze excess tyrosine to 4-hydroxyphenylpyruvate (4HPP) (Liu et al., 2018). Additionally, the mutation of the global transcription factor FruR (E173K), which controls the expression of FruR operator-containing genes coding key enzymes of virtually every major pathway of carbon metabolism, had no noticeable effect on *p*-coumaric acid titer (strain QZT018).

3.2. Strengthen the supply of malonyl-CoA

Malonyl-CoA is another key precursor for flavonoid biosynthesis. The shared core structure of flavonoids, naringenin, is biosynthesized by the condensation of one molecule of *p*-coumaroyl-CoA (produced by 4-coumarate-CoA ligase, 4CL) and three molecules of malonyl-CoA under the catalysis of chalcone synthase CHS and the assistance of chalcone isomerase-like protein CHIL, followed by the cyclization of the intermediate naringenin chalcone either under neutral conditions or with the assistance of chalcone isomerase CHI (Fig. 3a). In order to evaluate intracellular malonyl-CoA, we constructed naringenin producing strain QZT019 with co-expression of *At4CL1* from *Arabidopsis thaliana*, *PhCHIL* from *Petunia x hybrida*, *EbCHS* from *Erigeron breviscapus* and *ErCHI* from *Eubacterium ramulus*. When *p*-coumaric acid was fed at the beginning of fermentation, the engineered strain was capable of converting 200.00 mg/L *p*-coumaric acid into 133.10 mg/L naringenin (Fig. 3e, condition I). However, when the feeding of *p*-coumaric acid occurred at different times or in distributed supplements, naringenin production varied significantly. This may be caused by the dynamic changes in malonyl-CoA content in *E. coli* cells, since previous report showed that acyl-CoA concentrations within *E. coli* were mainly elevated during the logarithmic phase (0.05–1.50 nmol/(mg dry wt) of acetyl-CoA, and 0.01–0.23 nmol/(mg dry wt) of malonyl-CoA), but decreased to about 5% of the logarithmic phase levels during the stable phase (Takamura and Nomura, 1988). Hypothetically, it is essential to ensure adequate malonyl-CoA supply throughout the stationary phase for efficient synthesis of flavonoids.

In *E. coli*, malonyl-CoA is produced from acetyl-CoA through the catalysis of acetyl-CoA carboxylase ACC and mainly employed in fatty acid synthesis. Several strategies have been reported to increase intracellular malonyl-CoA production, including ACC gene overexpression (Wang et al., 2022b), introduction of the malonate assimilation pathway (Qiu et al., 2022), and inhibition of fatty acid synthesis genes (Fang et al., 2021) (Fig. 3b). To facilitate the evaluation of the intracellular malonyl-CoA pool, we initially established a reporter system in strain QZT020. This strain harbors the type III polyketide synthase *RppA*, capable of catalyzing the polymerization five molecules of malonyl-CoA into red pigment flaviolin (Fig. 3c). The absorbance of the supernatant at 340 nm demonstrates a linear correlation with intracellular malonyl-CoA levels, thus serving as a sensitive indicator of malonyl-CoA abundance within microbial cells (Yan et al., 2018). Subsequently, *CgACC* (Zhao et al., 2018) (comprising two subunit genes of *AccBC* and *DtsR1* from *Corynebacterium glutamicum*), *SeACC* (Wang et al., 2022b) (*SeAccABCD* gene from *Salmonella enterica*), the malonate assimilation pathway (Qiu et al., 2022) (*matB* gene coding malonyl-CoA synthetase and *matC* gene coding dicarboxylate carrier protein from *Rhizobium*

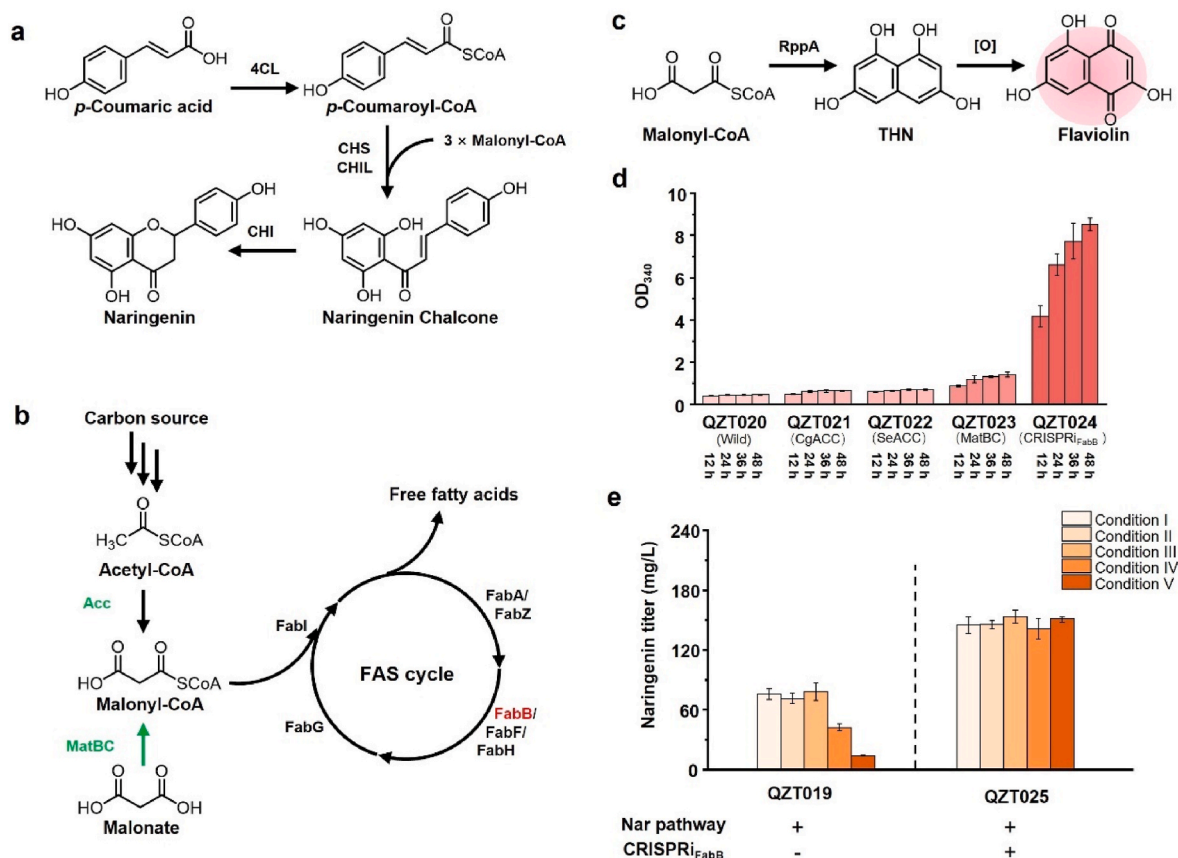


Fig. 3. Naringenin biosynthesis from *p*-coumaric acid. (a) Biosynthetic pathway from *p*-coumaric acid to naringenin. (b) Production and consumption pathways of malonyl-CoA in *E. coli*. Green: overexpression; Red: downregulation. (c) Flavioin biosynthesis from malonyl-CoA. (d) The OD₃₄₀ of the supernatant of engineered strains that enhance malonyl-CoA synthesis. (e) Production of naringenin within different precursor feeding conditions. Data shown are mean ± SD (n = 3 independent experiments). Condition I: Feeding 200.00 mg/L *p*-coumaric acid at 0 h; Condition II: Feeding 100.00 mg/L *p*-coumaric acid at 0 h and 100.00 mg/L *p*-coumaric acid at 12 h; Condition III: Feeding 100.00 mg/L *p*-coumaric acid at 0 h and 100.00 mg/L *p*-coumaric acid at 24 h; Condition IV: Feeding 100.00 mg/L *p*-coumaric acid at 0 h and 100.00 mg/L *p*-coumaric acid at 36 h; Condition V: Feeding 200.00 mg/L *p*-coumaric acid at 36 h.

trilobata), and the CRISPRi plasmid (capable of effectively down-regulating the 3-oxoacyl-[acyl carrier protein] synthase *fabB* involved in fatty acid synthesis) (Li et al., 2022b) were individually introduced into strain QZT020 to assess the efficacy of these strategies in enhancing cellular malonyl-CoA production.

The overexpression of *CgACC* (strain QZT021) and *SeACC* (strain QZT022) led to a moderate enhancement in malonyl-CoA abundance, with respective increments of 45% and 63% at 48 h (Fig. 3d). However, upon entry into the stationary phase (>12 h), there was no sustained increase in metabolic flux towards malonyl-CoA in *CgACC* or *SeACC* overexpression strains (QZT021 and QZT022). This observation is consistent with the reported substantial reduction of intracellular acyl-CoA during the stationary phase (Takamura and Nomura, 1988). Conversely, both the heterologous introduction of the malonate assimilation pathway (strain QZT023) and the downregulation of the fatty acid synthesis (strain QZT024) significantly increased metabolic flux towards malonyl-CoA and derived flavioin in the stationary-phase cells (Fig. 3d and Supplementary Fig. S2). The CRISPRi strategy yielded the highest metabolic flux towards malonyl-CoA and derived flavioin titer, which was ultimately 18.07 and 6.04 times higher than that of the original strain and the *matBC* overexpression strain, respectively.

Therefore, we elected to downregulate the *fabB* gene in the engineered strain QZT019 via CRISPRi, generating strain QZT025. As expected, the strain exhibited robust naringenin production upon supplementation with precursor *p*-coumaric acid, regardless of feeding variations (Fig. 3e). Moreover, co-cultivating QZT025 and QZT016 at an optimal inoculation ratio of 2:1 resulted in the *de novo* synthesis of

246.38 mg/L naringenin from glucose (Supplementary Fig. S3).

3.3. Establishment of flavonoid biosynthetic pathways

Flavonoids can be further categorized into four distinct classes depending on the structural features of the C ring: flavanones, flavones, flavanols, and flavonols (Fig. 4a and Supplementary Fig. S1). Initially, we established and optimized the heterologous biosynthetic pathways for representative compounds belonging to each of these four categories.

Synthesis of flavanones. The most representative flavanones isosakuranetin, eriodictyol and hesperetin, renowned for their diverse health benefits encompassing neurological, cardiac, hepatoprotective, anti-diabetic, anti-obesity and longevity gene-activating effects (Deng et al., 2020; Janyou et al., 2023; Maruyama et al., 2009; Yeh et al., 2022), can be synthesized through post-modification (methylation, hydroxylation) of the key precursor naringenin (Fig. 4b). In the pursuit of identifying the biosynthetic enzymes accountable for isosakuranetin and hesperetin, a comprehensive screening of regiospecific O-methyltransferases (OMTs) from diverse plants sources was undertaken. Specifically, nine OMT genes, namely *DcOMT6* from *Dianthus caryophyllus*, *SOMT2* from *Glycine max*, *CtOMT2* and *CtOMT3* from *Carthamus tinctorius*, *ShMOMT1* and *ShMOMT2* from *Solanum habrochaites*, *MpOMT4* from *Mentha x piperita*, *PaF4'OMT* from *Plagiochasma appendiculatum*, and *CsOMT* from *Citrus sinensis*, were individually expressed in *E. coli* MG1655(DE3), followed by supplementation with 200.00 mg/L naringenin or eriodictyol as substrate (Fig. 4c). Five of them, *CtOMT2*, *CtOMT3*, *MpOMT4*, *PaF4'OMT*, and *CsOMT*, demonstrated activities in

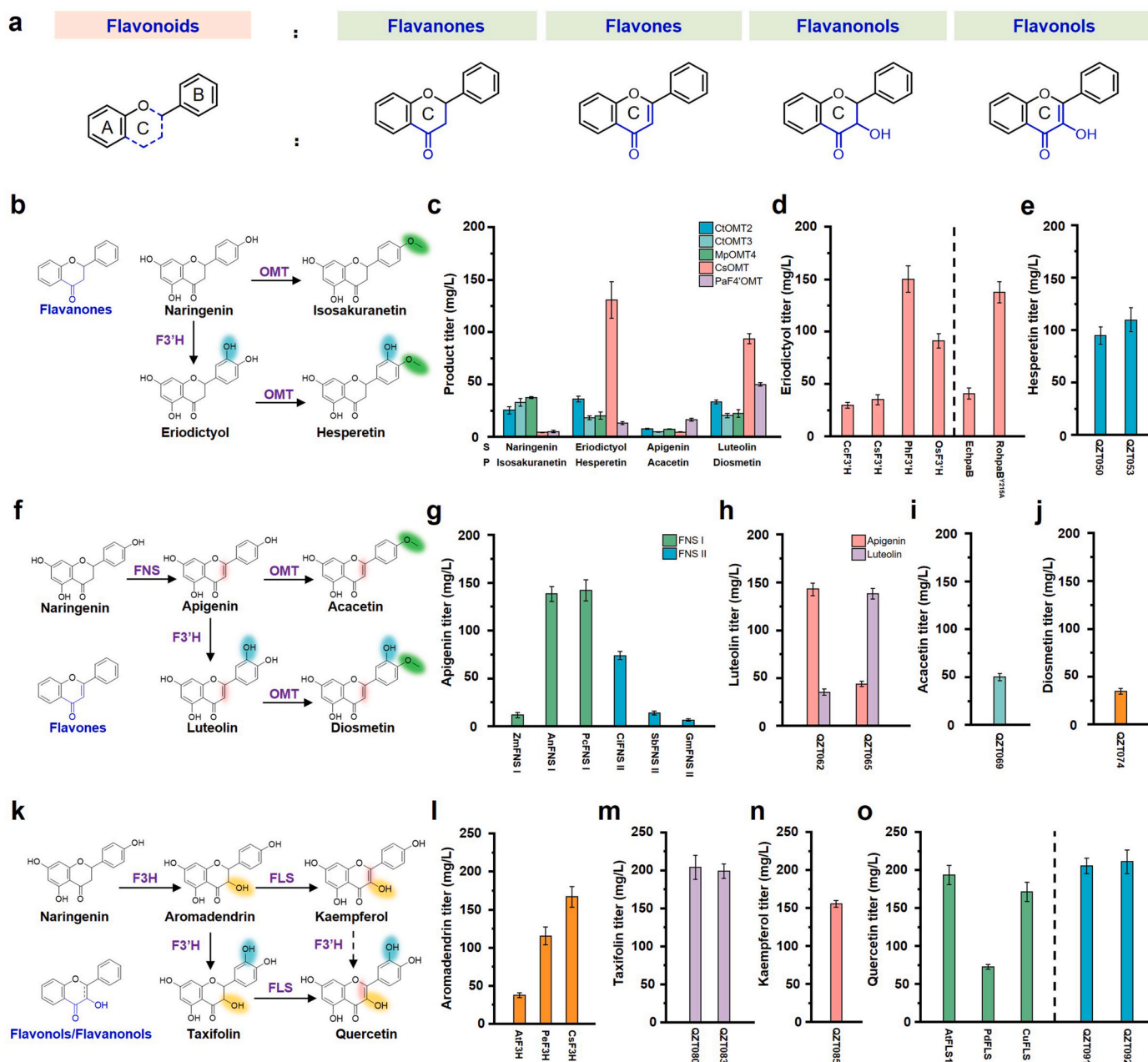


Fig. 4. Construction of flavonoids biosynthetic pathways. (a) Classification and core structure of flavonoids. (b) Flavonones biosynthetic pathway. (c) Biosynthesis of isosakuranetin, hesperetin, acacetin and diosmetin by expression of *CtOMT2*, *CtOMT3*, *MpOMT4*, *CsOMT* and *PaF4'OMT* using 200.00 mg/L substrate. S: Substrates; P: products. (d) Production of eriodictyol from 200.00 mg/L naringenin by expressing different flavonoid 3'-hydroxylase (F3'H). (e) Production of hesperetin from 200.00 mg/L naringenin. (f) Flavones biosynthetic pathway. (g) Biosynthesis of apigenin from 200.00 mg/L naringenin by expressing different flavone synthase (FNS). (h) Production of luteolin from 200.00 mg/L naringenin. (i) Production of acacetin from 200.00 mg/L naringenin. (j) Production of diosmetin from 200.00 mg/L naringenin. (k) Flavanolols and flavonols biosynthetic pathway. (l) Biosynthesis of aromadendrin from 200.00 mg/L naringenin by expressing different flavonoid 3-hydroxylase (F3H). (m) Production of taxifolin from naringenin. (n) Production of kaempferol from 200.00 mg/L naringenin. (o) Production of quercetin. Data shown are mean \pm SD (n = 3 independent experiments).

catalyzing the methylation of both naringenin and eriodictyol at the 4' hydroxy group of the B ring, leading to the production of isosakuranetin and hesperetin. Notably, the strain QZT028 harboring *MpOMT4* exhibited the highest production of isosakuranetin with a titer of 37.24 mg/L, while *CsOMT* demonstrated the highest level of hesperetin (132.01 mg/L).

Next, we proceeded to screen the flavonoid 3' hydroxylases (F3'H), which can be divided into two categories: cytochrome P450 and two-component flavin-dependent monooxygenase HpaBC. Cytochrome P450 collaborates with the highly conserved cytochrome P450

reductase (CPR) to facilitate various oxidative reactions. In this study, four plant-derived P450 (*CsF3'H* from *Citrus sinensis*, *CchF3'H* from *Callistephus chinensis*, *OsF3'H* from *Oryza sativa Japonica Group*, and *PhF3'H* from *Petunia x hybrida*) combined with three CPR (*AtCPR1* from *Arabidopsis thaliana*, *BtCPR* from *Beta vulgaris subsp. vulgaris*, and *LjCPR* from *Lotus japonicus*) were evaluated. Feeding 200.00 mg/L substrate assays demonstrated the ability of all P450s to recognize naringenin, with optimal catalytic activity observed when paired with *LjCPR* (Supplementary Fig. S4). The combination of *PhF3'H* and *LjCPR* (strain QZT043) yielded the highest eriodictyol titer, reaching 149.93 mg/L

(Fig. 4d). HpaB exhibits a broad spectrum of activity against phenolic compounds, converting flavonoids into 3'-hydroxylated counterparts. HpaC, a flavin-dependent oxidoreductase, supplies $\text{FADH}_2/\text{FMNH}^-$ to HpaB (Louie et al., 2003; Xun and Sandvik, 2000). In this study, we chose two distinct HpaB genes (*EcHpaB* from *E. coli* and *RoHpaB*^{Y215A} variant from *R. opacus* B4 (Wang et al., 2022a)) with coexpression of *EcHpaC* from *E. coli*. The expression of *RoHpaB*^{Y215A} (strain QZT048) efficiently synthesized 137.36 mg/L eriodictyol from naringenin, comparable to strain QZT043 (expressing *PhF3'H* and *LjCPR*) (Fig. 4d). Similar to the above tested P450-type F3'H, HpaB also displayed specific catalytic activity towards naringenin rather than isosakuranetin (Supplementary Fig. S5). This can be attributed to the formation of novel hydrogen bonds between Y215 and Y123 in the enzyme *RoHpaB*^{Y215A}, drawing the naringenin closer to the key catalytic site (Wang et al., 2022a). Additionally, the combinations of *PhF3'H/LjCPR* or *RoHpaB*^{Y215A}/*EcHpaC* also demonstrated robust catalytic activity with other flavonoids (Supplementary Fig. S6).

To facilitate the biosynthesis of hesperetin from naringenin, we incorporated the *CsOMT* gene into both the QZT049 and QZT054 strains, optimizing their expression levels via plasmids with varying copy numbers. Results showed that expressing *CsOMT* gene through medium copy-number vector is the most effective. The resultant strain QZT053 (expressing *CsOMT/RoHpaB*^{Y215A}/*EcHpaC*) exhibited enhanced production of hesperetin at 113.24 mg/L with 200.00 mg/L naringenin as substrate under the optimal condition, slightly outperforming QZT050 (expressing *CsOMT/PhF3'H/LjCPR*) which yielded 97.95 mg/L (Fig. 4e and Supplementary Fig. S7).

Synthesis of flavones. Flavones feature a double bond at the 2–3 positions of the C ring, which can be generated through oxidative desaturation. The representative flavone apigenin, notable for against cancer, cardiovascular diseases, arthritis, and diabetes (Ali et al., 2017), can be synthesized from naringenin through flavones synthase (FNS), followed by subsequent hydroxylation and methylation steps to generate other flavones such as luteolin, acacetin and diosmetin (Fig. 4f). Two distinct types of FNS, FNS I and FNS II, have been reported (Martens and Mithöfer, 2005). FNS I belongs to the 2-oxoglutarate dependent dioxygenase (2-OGDD) family within the cytoplasm (Martens et al., 2001), and FNS II is a membrane-bound NADPH-dependent P450 monooxygenase that collaborates with CPR to facilitate catalysis (Zheng et al., 2023). In our investigation, screening experiments were conducted involving three FNS I genes (*ZmFNS I* from *Zea mays*, *AnFNS I* from *Angelica archangelica*, and *PcFNS I* from *Petroselinum crispum*) and three FNS II genes (*CiFNS II* from *Chrysanthemum indicum*, *GmFNS II-2* from *Glycine max*, and *SbFNS II-1* from *Scutellaria baicalensis*) alongside the redox partner *LjCPR* to catalyze the conversion of naringenin into apigenin. As shown in Fig. 4g, 2-OGDD FNS I exhibited significantly higher apigenin yield compared to P450 FNS II with 200.00 mg/L naringenin as substrate, consistent with the inherent challenges associated with heterologous expression of plant P450 enzymes in *E. coli*. Particularly noteworthy was the strain QZT057 expressing *PcFNS I* displayed the highest apigenin production, reaching 142.70 mg/L. Furthermore, we co-expressed the preferred *PcFNS I* with the aforementionedly screened F3'H enzymes (*PhF3'H/LjCPR* and *RoHpaB*^{Y215A}/*EchpaC*) to construct synthetic pathways for the anticancer (Prasher et al., 2022; Tuli et al., 2022) flavone luteolin. And this was also followed by the fine-tuning of gene expression levels (Supplementary Fig. S8). The deployment of *RoHpaB*^{Y215A}/*EchpaC* via a high copy-number vector in tandem with *PcFNS I* expressed through a medium-copy number vector (strain QZT065) culminated in the highest luteolin yield (147.26 mg/L) with 200.00 mg/L naringenin as substrate, while concurrently minimizing the intermediate apigenin (43.89 mg/L) (Fig. 4h). In contrast, the co-expression involving *PhF3'H/LjCPR* and *PcFNS I* (strain QZT062) resulted in an obvious accumulation of the intermediate apigenin (152.02 mg/L) and a low luteolin output (35.27 mg/L). The intermediate accumulation in strain QZT062 may be attributable to the superior electron competition between FNS I and

F3'H, resulting in the diminished level of hydroxylation. Conversely, HpaBC, which relies on the $\text{FADH}_2/\text{FMNH}^-$ cofactor, remains unaffected by FNS I.

Acacetin and diosmetin are methylated flavones, notable for their wide-ranging therapeutic potential in addressing cancer, inflammation, infection, and a variety of metabolic disorders (Li et al., 2022a; Singh et al., 2020). To identify the biosynthetic enzymes, we fed 200.00 mg/L substrate apigenin and luteolin respectively into the fermentation medium of strains QZT026–QZT030, each expressing the above screened five methyltransferases (*CtOMT2*, *CtOMT3*, *MpOMT4*, *PaF4'OMT*, and *CsOMT*) capable of catalyzing the methylation at the 4' hydroxy group of the B ring. Results showed that strains harboring *PaF4'OMT* and *CsOMT* produced the highest yields of acacetin (15.95 mg/L) and diosmetin (94.36 mg/L), respectively (Fig. 4c). Through further refinement of gene combinations and optimization of expression levels, we achieved a production yield of 49.35 mg/L acacetin from 200.00 mg/L naringenin by expressing *PaF4'OMT* with a low-copy plasmid and *PcFNS I* with a high-copy plasmid in strain QZT069 (Fig. 4i and Supplementary Fig. S9). Similarly, a production yield of 34.22 mg/L diosmetin was attained by expressing *CsOMT* and *PcFNS I* with a medium-copy plasmid and *RoHpaB*^{Y215A}/*EchpaC* with a high-copy plasmid in strain QZT074 (Fig. 4j and Supplementary Fig. S10).

Synthesis of flavanonols. Flavanonols, derived from flavanones through hydroxylation at the 3-position of the C ring catalyzed by flavanone 3-hydroxylase (F3H), play a crucial role in various therapeutic applications. Aromadendrin, a representative flavanone synthesized from naringenin by F3H (Fig. 4k), is particularly notable for its hepatoprotective effects against acetaminophen-induced liver damage via SIRT1 pathway activation (Zhang et al., 2021). Aromadendrin undergoes further hydroxylation by F3'H, yielding the flavanone taxifolin, an investigational therapeutic for Alzheimer's disease and cerebral amyloid angiopathy (Saito et al., 2021). In our previous study, we successfully synthesize kaempferol from naringenin by fusing three F3H genes (*AtF3H* from *Arabidopsis thaliana*, *PeF3H* from *Populus euphratica*, and *CsF3H* from *Citrus sinensis*) with FLS (Qiu et al., 2022). In this study, we further evaluated the activities of these three F3Hs for aromadendrin synthesis, revealing that the *CsF3H* enzyme exhibited the highest activity, yielding 166.52 mg/L of aromadendrin from 200.00 mg/L naringenin (Fig. 4l). Optimal expression of the *CsF3H* gene via a medium copy-number vector was found to be most effective for product biosynthesis (Supplementary Fig. S11). Furthermore, the highest taxifolin production (203.45 mg/L) was achieved by combining *CsF3H* with *PhF3'H/LjCPR* (strain QZT080) with 200.00 mg/L naringenin as substrate, slightly surpassing the combination of *CsF3H* with *RoHpaB*^{Y215A}/*EchpaC* (198.27 mg/L, strain QZT083) (Fig. 4m). Interestingly, the conversion rate of naringenin to taxifolin by F3H and F3'H enzymes is observed to be higher than that of naringenin to aromadendrin catalyzed by F3H alone. This phenomenon could be attributed to the substrate promiscuity of the enzymes: naringenin can be either hydroxylated by F3H to aromadendrin, subsequently by F3'H to taxifolin, or undergo the reverse catalytic sequence through intermediate eriodictyol to generate taxifolin (Supplementary Fig. S12). Consistently, further efficacy tests demonstrated the synergistic effect of F3H and F3'H in directing the metabolic flux toward taxifolin synthesis.

Synthesis of flavonols. Flavonols are synthesized from flavanols through the oxidative desaturation catalyzed by flavonol synthase (FLS) (Fig. 4k). Kaempferol, derived from aromadendrin, is celebrated for its anti-inflammatory properties, offering therapeutic potential for acute and chronic inflammation (Ren et al., 2019). Our previous research identified the optimal enzymes for kaempferol synthesis (Qiu et al., 2022). Utilizing a combination of *PeF3H* and *PdFLS*, we achieved a synthesis yield of 155.28 mg/L kaempferol with 200.00 mg/L naringenin as substrate (Fig. 4n). Quercetin, another flavonol derived from taxifolin, boasts significant lipophilicity, facilitating its traversal of the blood-brain barrier and offering prophylaxis against neurodegenerative ailments (Deepika and Maurya, 2022). In pursuit of optimal quercetin

synthesis, we evaluated three FLS genes (*AtFLS1* from *Arabidopsis thaliana*, *PdFLS* from *Populus deltoides* and *CuFLS* from *Citrus unshiu*) and found that the *AtFLS1* enzyme exhibited the highest activity, yielding 192.41 mg/L quercetin from 200.00 mg/L taxifolin (Fig. 4o). Subsequently, we introduced *AtFLS1* into the combinations of *CsF3H* with *RoHpaB*^{Y215A}/*EchpaC* or *PhF3H*/*LjCPR*, followed by optimization of gene expression levels (Supplementary Fig. S13). Expressing *RoHpaB*^{Y215A} or *PhF3H* through a high-copy number vector, along with *CsF3H* and *AtFLS1* through low copy number vector, proved to be the most effective. Consequently, with 200.00 mg/L naringenin as substrate, the engineered strains QZT091 and QZT092 achieved the highest quercetin production of 204.68 mg/L and 209.97 mg/L, respectively (Fig. 4o).

3.4. Metabolic division engineering of *E. coli* co-cultures for flavonoids biosynthesis

Flavonoids, complex natural compounds with intricate metabolic pathways, often pose significant metabolic burdens and yield limitations when synthesized *de novo* by a single engineered *E. coli* strain (Liu et al., 2022a; Qiu et al., 2022). To address these challenges, we established microbial co-culture systems to balance cell growth and product synthesis.

Previous studies have shown that *p*-coumaroyl-CoA exerts feedback inhibition on TAL, while flavonoid pathway products alleviate cellular toxicity by non-competitive inhibiting CHS (Peters et al., 1988; Santos et al., 2011; Whitehead and Dixon, 1983). To mitigate these inhibitory

effects, we partitioned TAL and *p*-coumaroyl-CoA into distinct sub-populations, as well as CHS and flavonoid products, to establish a type I co-culture system (linear metabolic distribution approach). This system comprised three strains, containing synthetic modules for *p*-coumaric acid, naringenin and flavonoids, respectively (Fig. 5a and Table S4). Under the optimal inoculation ratio (1:1:1), the engineered *E. coli* consortia successfully achieved *de novo* synthesis of flavonoid products (Fig. 5e and Supplementary Fig. S14). Notably, production efficiency testing demonstrated that the type I co-culture system is more efficient than the commonly used single culture strategy with the entire biosynthetic pathway (Supplementary Fig. S15).

The U-shaped metabolic distribution strategy separates upstream and downstream modules from midstream modules, effectively alleviating inhibitory interactions between pathways. Compared to the type I co-culture system, the U-shaped approach requires fewer sub-populations, simplifies the co-culture system, and optimizes resource allocation and utilization, making it a highly promising strategy for co-culture applications. A similar strategy was previously employed by us to efficiently synthesize kaempferide (Qiu et al., 2022). Building on this foundation, we further explored the potential of the U-type metabolic distribution method. Using *p*-coumaric acid and naringenin as metabolic division nodes, we incorporated the flavonoid synthesis module into the *p*-coumaric acid-producing strain QZT110, generating strains QZT112-QZT127. These strains were then co-cultured with strain QZT111 (containing the naringenin synthesis module) to establish a U-shaped type II co-culture system (Fig. 5b and Table S4). Following

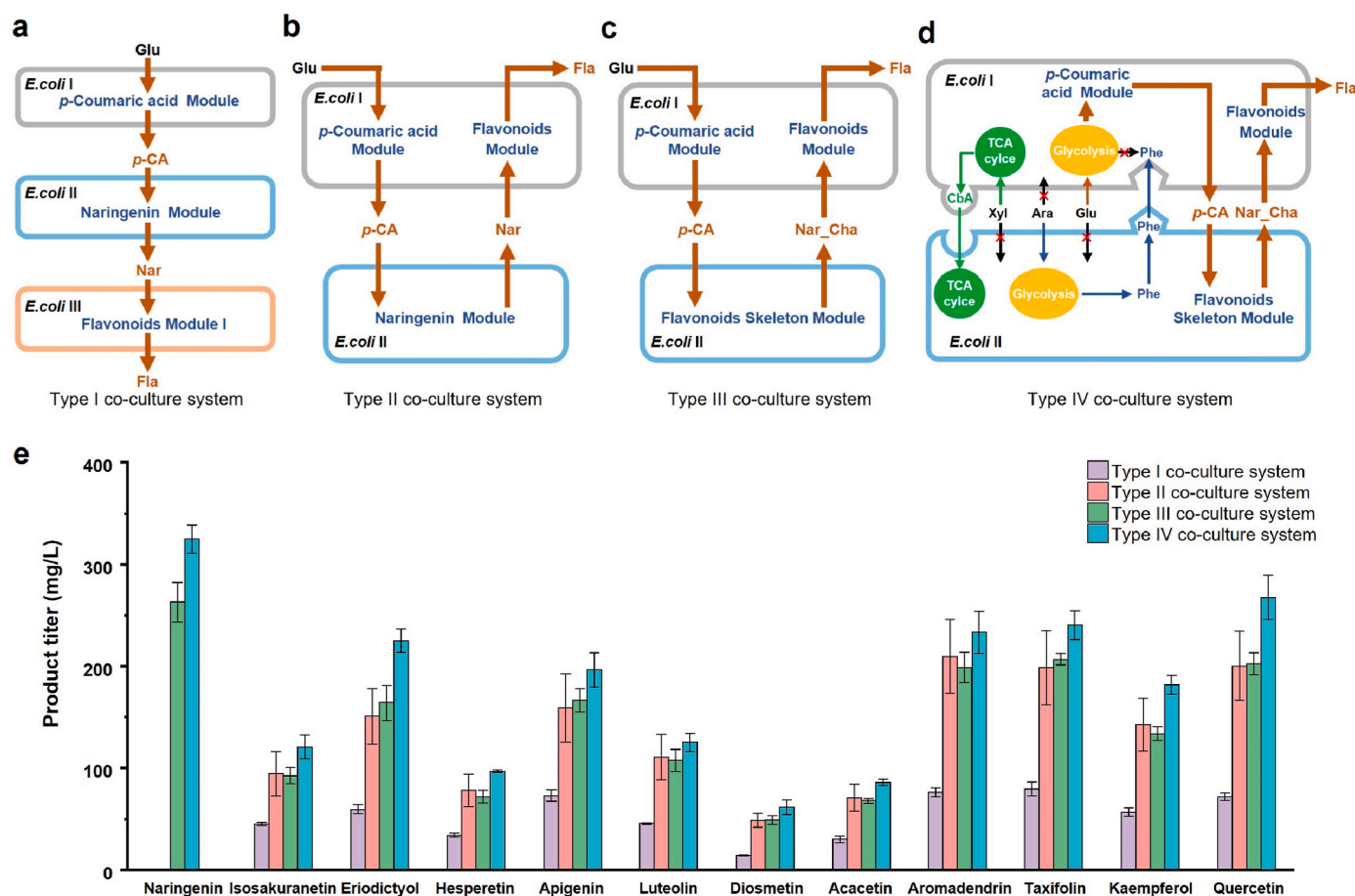


Fig. 5. Flavonoids biosynthesis by *E. coli* co-culture systems. (a) Type I co-culture system with three-bacterial linear division. (b) Type II co-culture system with U-shaped division using *p*-coumaric acid and naringenin as node compounds. (c) Type III co-culture system with U-shaped division using *p*-coumaric acid and naringenin chalcones as node compounds. (d) Type IV co-culture system with obligate mutualism. (e) The titer of flavonoids in different co-culture systems. Data shown are mean \pm SD ($n = 3$ independent experiments). Strains used in co-culture systems were listed in the Supplementary Table S4 *p*-CA: *p*-coumaric acid; Nar: naringenin; Nar_Cha: naringenin chalcone; Fla: flavonoids; CbA: carboxylic acid; Xyl: xylose; Ara: arabinose; Glu: glucose; Phe: phenylalanine.

optimization of the inoculation ratio (2:1), the newly established co-culture system achieved significantly higher productions (2.1–3.4 fold) than the linear type I co-culture system (Fig. 5e and Supplementary Fig. S16), demonstrating its advantage and universality. Interestingly, the co-culture system involving *RoHpaB*^{Y215A}/*EcHpaC* exhibited higher flavonoid production than *PhF3H*/*LjCPR*. Further investigation revealed that introducing *LjCPR* to the *p*-coumaric acid-producing strain significantly reduced the production *p*-coumaric acid (Supplementary Fig. S17), suggesting potential competing pathways were likely activated or upregulated by this redox protein, thereby resulting in insufficient supply of precursors. Therefore, selecting *RoHpaB*^{Y215A}/*EcHpaC* instead of *PhF3H*/*LjCPR* as the 3' hydroxylase in the U-shaped co-culture system is more favorable for flavonoid synthesis in *E. coli*.

To further assess the potential impact of selecting different node compounds in the downstream module on the final product yield, we alternative redistributed the naringenin synthesis step into the flavanone synthesis module and established the U-shaped type III co-culture system (QZT129–QZT140 with QZT141) (Fig. 5c and Table S4), using naringenin chalcone as the metabolic splitting node. This metabolic division strategy yielded similarly effective results as the type II co-culture system (Fig. 5e and Supplementary Fig. S18), confirming the robustness of the U-shaped division methodology and highlighting the potential for rational design and selection of metabolic splitting nodes. The initial inoculation ratio significantly influenced both the final population distribution and the product titer. At the optimal inoculation ratio of 2:1, the flavonoid skeleton synthesis strain accounted for 59% of the population at 48 h, showing a marked difference compared to the population ratios observed at other inoculation ratios (40%, 70%, 76%, and 85%) (Supplementary Figs. S19a–e). Flavonoid yields also varied substantially across different inoculation ratios (Supplementary Fig. S18). These results underscore that while the neutral microbial consortia effectively facilitate division of labor and collaboration in synthesizing complex flavonoids, their inherent instability requires external regulation to fully unlock their potential.

For strains in the co-culture systems, the pathways of *p*-coumaric acid synthesis and the tricarboxylic acid (TCA) cycle share crucial intermediates such as phosphoenolpyruvate (PEP), pyruvate (PYR), and acyl-CoA (Soma et al., 2014). These overlapping utilizations can lead to competition, impacting cell growth and metabolic balance (Peng et al., 2004). Further investigations showed that variations in inoculation ratios significantly affected flavonoid production (Supplementary Figs. S16 and S18), revealing the instability and environmental sensitivity of the non-interactive *E. coli* co-culture systems. To address this challenge, we established obligate mutualistic relationships between *E. coli* strains, employing orthogonal carbon sources and facilitating multiple metabolite cross-overs to enhance system stability. We decoupled the pentose phosphate and glycolytic pathways from the TCA cycle to stabilize the metabolite production without compromising growth potential. To eliminate unpredictable shifts in metabolic regulation, we disrupted all the connections between glycolysis and the TCA cycle (via *pykA*, *pykF*, *eda*, *ppc*, *pck*, and *ppsA* knockouts), resulting in strains QZT142 (derived from QZT110) and QZT143 (derived from MG1655 (DE3)) (Supplementary Figs. S20 and S21). Post-metabolic engineering, strains QZT142 (with addition of 0.50 g/L phenylalanine) and QZT143 exhibited no growth in glucose minimal medium but regained the growth upon supplementation with CbA from the TCA cycle (Supplementary Figs. S22a and c), demonstrating the successful decoupling of the pentose phosphate and glycolytic pathways from the TCA cycle. To directly synthesize necessary carboxylic acid intermediates from xylose, we blocked the arabinose utilization pathway by deleting *araABCD* and introduced the *Dahms* pathway (Fujiwara et al., 2020), which directly flows towards the TCA cycle, into QZT142, resulting in strain QZT144 (Supplementary Fig. S23a). Strain QZT144, derived from strain QZT142, which was phenylalanine deficient, could not grow in the presence of phenylalanine with glucose or xylose, but the growth was recovered only in the presence of xylose, glucose, and

phenylalanine (Supplementary Fig. S22b), and high *p*-coumaric acid was produced (543.86 mg/L). We further severed the glucose and xylose utilization pathways of QZT143 to generate strain QZT145. It failed to grow with xylose and glucose as carbon source and addition of CbA, but resume the growth only when arabinose and exogenous carboxylic acid intermediates were provided (Supplementary Figs. S22d and S23b). QZT145 shared the symbiotic partnership with QZT144 (Supplementary Fig. S22e). Specifically, QZT144 utilized glucose for metabolite synthesis, xylose for carboxylic acid synthesis, and supplied carboxylic acids to QZT145, while QZT145 utilized arabinose and supplied phenylalanine to QZT144 (Fig. 5d).

Subsequently, we integrated the different flavonoid synthesis modules into strain QZT144, yielding serial strains QZT158–QZT169, and the naringenin chalcone synthesis module into strain QZT145, yielding strain QZT170. Co-culturing one of strains QZT158 to QZT169 (*E. coli* I) with QZT170 (*E. coli* II) generated type IV co-culture system with a symbiotic relationship among strain members (Fig. 5d and Table S4). Remarkably, despite varying inoculation ratios ranging from 4:1 to 1:4, the co-culture system exhibited strong robustness throughout the 48-h fermentation, with the flavonoid skeleton-synthesizing strain comprising 51%–60% of the population (Supplementary Figs. S19f–j). This robust system achieved higher yields of flavonoids, with fluctuations in target compound production significantly smaller than those observed in the neutral co-culture system under varying initial inoculation ratios (Fig. 5e and Supplementary Table S4 and Fig. S24). These results highlight the stabilizing effect of the symbiotic relationship and its positive impact on the production of flavonoids. Furthermore, the synthesis of isosakuranetin, hesperetin, luteolin, diosmetin, and acetin was accompanied by the accumulation of byproducts, which were attributed to the limited catalytic efficiency of pathway enzymes (Supplementary Table S5). Nevertheless, the metabolic flow remained efficient, ensuring smooth synthesis of the target compounds.

3.5. Development of flavonoid glycoside biosynthetic module

The above findings comprehensively demonstrated the enhanced production efficiency of flavonoids by metabolic division engineering of co-culture system. We further explored the efficacy of this approach for the biosynthesis of flavonoid glycosides, including flavonoid-7-glucosides (flavonoid-Glus) and flavonoid-di-glycosides such as flavonoid-7-rutinosides (flavonoid-Ruts) and flavonoid-7-neohesperidoside (flavonoid-Neos). We established and optimized the flavonoid glycoside biosynthetic module (Fig. 6a), focusing on enhancing of sugar donor availability and screening for essential glycosyltransferase components.

Enhancing sugar donor supply. Flavonoid glycosides are synthesized through glycosyltransferase-catalyzed transfer of NDP/dNDP-sugar to specific positions on flavonoid compounds (Fig. 6a). In order to enhance the supply of sugar donors, we conducted a series of engineering modifications (Supplementary Fig. S25). The biosynthesis of flavonoid-Ruts and flavonoid-Neos requires glucose and rhamnose donors. Both of UDP-rhamnose and dTDP-rhamnose can serve as donors for rhamnosylation (Jiang et al., 2021). We established and evaluated the biosynthetic pathways for these two rhamnose donors. Three plant-derived potential UDP-rhamnose synthase coding genes (*AtRHM2* from *Arabidopsis thaliana*, *CsRHM* from *Citrus sinensis*, and *CsRHMB* from *Camellia sinensis*) and the endogenous dTDP-rhamnose synthesis pathway *rfaABCD* (comprising dTDP-glucose pyrophosphorylase gene *rfaA*; dTDP-glucose-4,6-dehydratase gene *rfaB*; dTDP-4-dehydrorhamnose-3,5-epimerase gene *rfaC* and dTDP-4-dehydrorhamnose-reductase gene *rfaD*) (Klena and Schnaitman, 1993) were individually co-expressed with the previously characterized rhamnosyltransferase (RhaT) gene *CmI*,2-RhaT (from *Citrus maxima*) (Ohashi et al., 2016; Xiao et al., 2023) to assess their effects on the biosynthesis of the target product naringin (naringenin-Neo) from substrate naringenin-7-glucoside (naringenin-Glu). Results showed that the introduction of UDP-rhamnose synthase was more effective compared

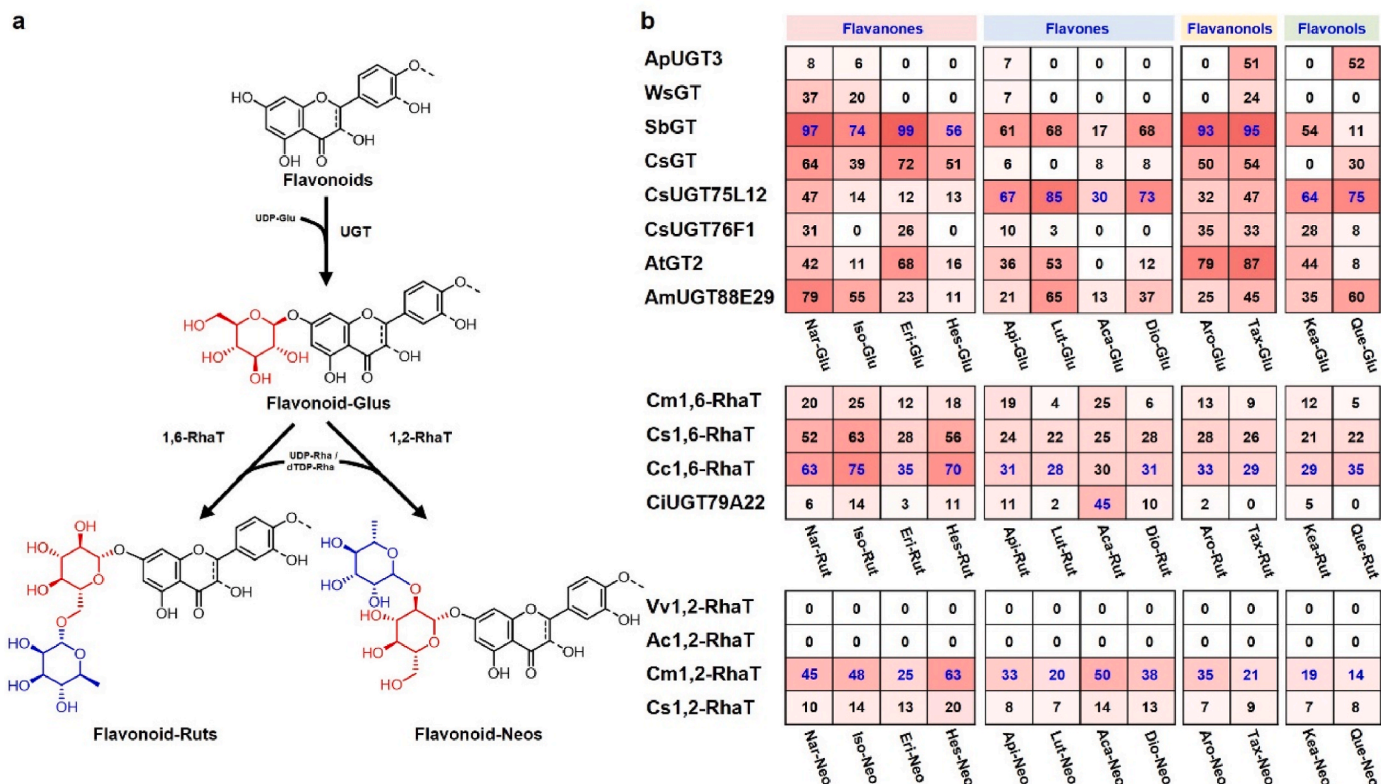


Fig. 6. Flavonoid glycosides biosynthesis and glycosyltransferases screening. (a) Biosynthetic pathway of flavonoid glycosides. (b) Screening of UGTs and RhaTs. The UGTs were screened using flavonoids as substrates, whereas the screening of RhaTs employed flavonoid-Glus as substrates. The numbers represent the conversion rate (%). Data shown are mean \pm SD ($n = 3$ independent experiments). Nar: Naringenin; Eri: Eriodictyol; Iso: Isosakuranetin; Hes: Hesperetin; Api: Apigenin; Lut: Luteolin; Aca: Acacetin; Dio: Diosmetin; Aro: Aromadendrin; Tax: Taxifolin; Kea: Kaempferol; Que: Quercetin; -Glu: 7-Glucoside; -Rut: 7-Rutinoside; -Neo: 7-neohepsidoside.

to the *rfbABCD* pathway (Supplementary Fig. S26). Among the UDP-rhamnose synthases tested, CsRHMB exhibited the highest efficacy, with strain QZT172 producing 61.22 mg/L of naringin. Further co-expression of *rfbABCD* and *CsRHMB* (strain QZT175) did not lead to an enhancement in naringin production. Additionally, the overexpression of *rfbABCD* had a modest impact on the endogenous metabolism of *E. coli*, resulting in a reduced growth rate (Supplementary Fig. S27), potentially influencing product yield.

UDP-glucose, the glucosyl donor for glucoside biosynthesis as well as the precursor for other sugar donors such as UDP-rhamnose, is frequently considered the bottleneck in the biosynthesis of heterologous glycosylated products (Xu et al., 2022; Yan et al., 2024). To enhance UDP-glucose supply, we knocked out the 5'-nucleotidase/UDP-sugar hydrolase *ushA* gene (Guo et al., 2022), whose absence would block UDP-glucose hydrolysis. Using naringin as the test target, the engineered strain QZT176 achieved a yield of 88.52 mg/L (Supplementary Fig. S28). Subsequently, we overexpressed the *pgm* (phosphoglucosyltransferase) and *galU* (UTP-glucose-1-phosphate uridylyltransferase) genes to further enhance UDP-glucose synthesis. The resultant strain QZT177 synthesized 112.42 mg/L of naringin, representing a 27% increase. Further introduction of *ugpA* (an isozyme gene of *galU*) from *Bifidobacterium bifidum*, the strain QZT178 exhibited an additional 5% increase (116.77 mg/L).

The glucose-1-phosphate (G1P) synthesis pathway diverts precursor glucose-6-phosphate (G6P) from glycolysis metabolism towards UDP-sugar biosynthesis (Supplementary Fig. S25), potentially impairing normal cellular metabolism (Mao et al., 2006). Introduction of an efficient heterologous NDP-sugar biosynthesis pathway in microorganisms utilizing diglycosides or polyglycosides presents a promising strategy for enhancing glucosyl donors (Feng et al., 2020). Sucrose synthase (SUS)

facilitates the reversible transfer of the glucose moiety between sucrose and nucleoside diphosphate (NDP) (sucrose + NDP \leftrightarrow NDP-glucose + fructose) (Huang et al., 2016). G6-amylase degrades long-chain dextrans into maltodextrin, which are then assimilated and metabolized by *E. coli* to yield G1P (Ruprecht et al., 2019). Similarly, cellobiose phosphorylase (Cep) breaks down cellobiose into glucose and G1P (Cabulong et al., 2021). Accordingly, we heterologously expressed and evaluated the effectiveness of the three types of enzymes, including GmSUS from *Glycine max*, G6-amylase from *Bacillus* sp. 707 and Cep94A from *Saccharophagus degradans* (Supplementary Fig. S25). The strains were cultured under conditions with corresponding sugars as carbon sources. Expression of Cep94A (strain QZT181) or G6-amylase (strain QZT180) significantly increased naringin production. Notably, Cep94A exhibited the highest effectiveness, yielding 191.41 mg/L, representing a 64% increase (Supplementary Fig. S29). These findings comprehensively demonstrated the efficacy of introducing heterologous pathways to enhance sugar donor supply. Through these metabolic engineering modifications, an enhanced supply of sugar donors was achieved.

Glycosyltransferase Screening. In order to biosynthesize flavonoid glycosides, we conducted screening for crucial UDP-glucuronosyltransferases (UGTs) and Rhamnosyltransferases (RhaTs). We selected and expressed eight potential plant-derived 7-O-UGTs (strains QZT182-QZT189) to assess their glycosylation activity with flavonoid substrates. These enzymes displayed significant substrate promiscuity towards flavonoids (Fig. 6b). Our screening efforts successfully identified glycosyltransferases with preferences for catalyzing the glycosylation of different types of flavonoids. Particularly noteworthy, SbGT from *Scutellaria baicalensis* demonstrated good glycosylation activity towards flavanones and flavanols, while CsUGT75L12 from *Camellia sinensis* showed proficiency in glycosylating flavones and

flavonols.

Subsequently, eight strains (QZT181, QZT190–QZT196) were individually engineered by overexpression of four 1,2-RhaTs and four 1,6-RhaTs. The substrate specificity and catalytic efficiency of these potential RhaTs were evaluated by feeding flavonoid glucoside substrates. For 6'-rhamnosylation, both Cc1,6-RhaT from *Citrus x clementina* and Cs1,6-RhaT from *Citrus sinensis* exhibited broad catalytic activity towards flavonoid-Glus, with Cc1,6-RhaT demonstrating higher catalytic efficiency (Fig. 6b). CiUGT79A22 from *Chrysanthemum indicum* displayed specific but elevated activity towards the substrate acetin-Glu. For 2'-rhamnosylation, both Cm1,2-RhaT from *Citrus maxima* and Cs1,2-RhaT from *Citrus sinensis* showed notable activity for biosynthesis flavonoid-Neos, with Cm1,2-RhaT demonstrating the broadest and highest

catalytic efficiency. These efficient glycosyltransferases identified through our screening process were subsequently employed to construct biosynthetic modules for producing flavonoid glycosides.

3.6. Metabolic division engineering of *E. coli* co-cultures for flavonoid glycosides biosynthesis

To achieve *de novo* synthesis of flavonoid glycosides, we developed the type V co-culture system (Fig. 7a) by integrating the flavonoid glycoside-producing strain into the previously constructed type IV coculture system. Similarly, a finely tuned obligate mutualistic interaction system was established among the three strains comprising the co-culture system. Specifically, we further introduced serine and glycerol

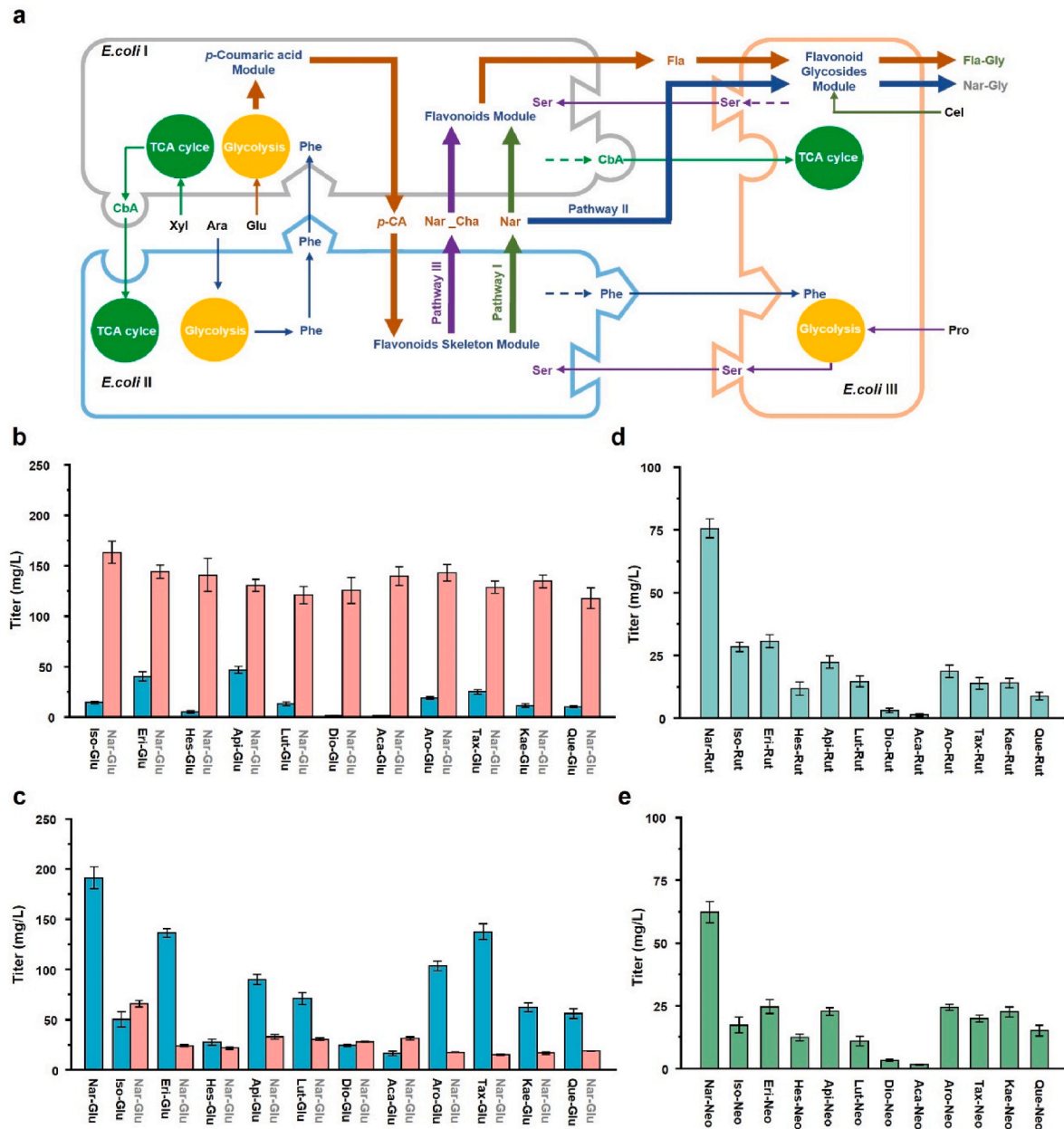


Fig. 7. Flavonoid glycosides biosynthesis by *E. coli* co-culture systems. (a) Metabolic engineering of obligate mutually beneficial type V co-culture system for *de novo* production of flavonoid-Glys. (b) The yields of flavonoid-Glus by the metabolic engineering of obligate mutually beneficial type V co-culture system with *p*-coumaric acid and naringenin as nodes. (c) The yields of flavonoid-Glus with *p*-coumaric acid and naringenin chalcone as nodes. (d) The yields of flavonoid-Ruts with *p*-coumaric acid and naringenin chalcone as nodes. (e) The yields of flavonoid-Neos with *p*-coumaric acid and naringenin chalcone as nodes. Data shown are mean \pm SD ($n = 3$ independent experiments). Strain information for the co-culture systems was provided in the [Supplementary Tables S6–S8](#). Pro: propane-1,2,3-triol; Cel: cellobiose; Ser: serine; Fla-Gly: flavonoid-7-glycoside; Nar-Gly: naringenin-7-glycoside.

utilization deficiency in *E. coli* I and II by knocking out the *serA* (coding phosphoglycerate dehydrogenase) (Li et al., 2022b) and *glpK* (coding glycerol kinase) (Li et al., 2022c). Concurrently, *E. coli* III was engineered to utilize propane-1,2,3-triol as the carbon source, and to be deficient in both phenylalanine and carboxylic acids (strain QZT210, Supplementary Fig. S30). Consequently, *E. coli* I (deficient in phenylalanine and serine) metabolized glucose to synthesize metabolites and utilized xylose to produce carboxylic acids. These carboxylic acids were supplied to both *E. coli* II (deficient in carboxylic acids and serine) and *E. coli* III (deficient in carboxylic acids and phenylalanine). *E. coli* II metabolized arabinose and provided phenylalanine to *E. coli* I and III, while *E. coli* III utilized propane-1,2,3-triol and supplied serine to the other two strains (Fig. 7a and Supplementary Figs. S31a–d).

Based on the glycosyltransferase screening results (Fig. 6b), we employed strain QZT211 (expressing *SbGT*) for synthesizing flavanone-Glus and flavanol-Glus, and strain QZT212 (expressing *CsUGT75L12*) for flavone-Glus and flavonol-Glus. Each of these strains were co-cultured with the flavonoid-producing strains to achieve *de novo* synthesis of flavonoid-Glus (Supplementary Table S6). Employing *p*-coumaric acid, naringenin, and the target flavonoid as division node compounds (Fig. 7a pathway I), the co-culture system exhibited a significant accumulation of the glucoside product of the intermediate naringenin (naringenin-Glu), with minimal amounts of target flavonoid-Glus (Fig. 7b). The target flavonoid-Glu was produced at a very low level, with minimal accumulation of other flavonoid intermediates or their corresponding glycosides (Fig. 7b and Supplementary Table S7). This indicated that the intermediate naringenin produced in *E. coli* II was directly captured by the glycosylation machinery in *E. coli* III (Fig. 7a pathway II). To address this issue, we replaced naringenin with naringenin-chalcone as the node compound (Fig. 7a pathway III). This adjustment notably reduced the production of naringenin-Glu and substantially enhanced the production of the target flavonoid-Glus (Fig. 7c and Supplementary Fig. S32 and Table S7). Especially, the co-culture system designed for the synthesis of Eri-Glu, Aro-Glu, and Tax-Glu produced substantial amounts of the target compounds (>130 mg/L), with minimal accumulation of Nar-Glu (<25 mg/L) (Supplementary Table S7). And the co-culture system for synthesizing Api-Glu, Kae-Glu, and Que-Glu also achieved significant accumulation of the corresponding flavonoids (50–60 mg/L) (Supplementary Table S7). In the stable condition after 48 h of fermentation, strain I of the three-strain consortia constituted approximately 40%–45% of the bacterial community, while strains II and III accounted for 25%–35% each, demonstrating high robustness (Supplementary Fig. S33). Notably, an initial inoculation ratio closely matching the stable community composition led to shorter cell density establishment times, faster progression to the plateau phase (Supplementary Fig. S33), and higher production of the target compounds (Supplementary Fig. S32). These results highlight the importance of rational metabolic division engineering in developing co-culture systems to overcome pathway promiscuity and by-product accumulation. By distributing competing pathways and precursors across different co-culture sub-populations, the metabolic flux can be effectively redirected towards the target products.

Furthermore, we employed the type V co-culture system to synthesize flavonoid-di-glycosides using the screened Cm1,2-RhaT and Cc1,6-RhaT (Supplementary Table S8). As anticipated, the three-bacteria co-culture system successfully achieved the *de novo* biosynthesis of 12 flavonoid-Ruts and 12 flavonoid-Neos for the first time, with Nar-Neo and Nar-Rut achieving the highest yields of 75.52 mg/L and 62.23 mg/L, respectively (Fig. 7d and e).

3.7. Expanding the co-culture system for synthesizing isoflavonoid, dihydrochalcone and glycosides

To further investigate the potential of the metabolic division engineering based co-culture system, we extended the strategy for the biosynthesis of other polyphenolic compounds (such as the isoflavonoid

and dihydrochalcone) and glycosides (Fig. 8a and b). We replaced the flavonoid synthesis module with the isoflavonoid synthesis module for the *de novo* production of genistein and its glycosides. We previously established the *de novo* biosynthetic pathway of genistein in *E. coli* (Liu et al., 2022a). To further achieve the synthesis of glycosylated products, we also screened the UGTs and RhaTs obtained in this study, and identified the enzymes (AmUGT88E29 from *Astragalus membranaceus*, Cc-1,6RhaT and Cm-1,2RhaT) with relatively high activities (Fig. 8c). Following the metabolic division engineering principles of U-shaped obligate mutualistic co-culture system, we distributed the genistein synthesis module and the *p*-coumaric acid synthesis module into one *E. coli* strain, and the flavonoid skeleton synthesis module into another strain (Supplementary Fig. S34). Remarkably, this balanced distribution resulted in an enhanced genistein production, achieving 66.58 mg/L, 2-fold of the yield compared to the previous report (Fig. 8d and Supplementary Table S4). With subsequent incorporation of individual glucoside-, rutoside-, and neohesperidoside-synthesizing strains, the co-culture system achieved the *de novo* production of 75.24 mg/L genistein-Glu, 6.24 mg/L genistein-Rut and 4.85 mg/L genistein-Neo, respectively (Fig. 8d and Supplementary Tables S6–S8).

We further substituted the chalcone isomerase (CHI) in the naringenin biosynthetic route with the ene reductase (CaER) from *Clostridium acetobutylicum*, establishing the *de novo* biosynthesis pathway of the dihydrochalcone phloretin (Liu et al., 2022b) (Supplementary Fig. S35). Using *p*-coumaric acid as the metabolic separation node, the fine-tuned co-culture system successfully achieved the *de novo* production of 3.50 mg/L of phloretin (Fig. 8e and Supplementary Table S4). Phloretin-glycosides have great potential as safe artificial sweeteners (flavor enhancers) with high sweetness and low calorie (Eichenberger et al., 2017). By individual introduction of the strains with glucoside-, rutoside-, and neohesperidoside-synthesizing modules, the fine-tuned co-culture system enabled the *de novo* production of 12.89 mg/L phloretin-Glu (trilobatin), 1.07 mg/L phloretin-Neo (naringin dihydrochalcone), and 1.32 mg/L phloretin-Rut, respectively (Fig. 8e and Supplementary Tables S6–S8).

4. Conclusions

Many natural products have intricate biosynthetic pathways. Eukaryotes have evolved intracellular compartmentalization to efficiently synthesize complex metabolites (Du and Li, 2021; Wang et al., 2024a; Zhang et al., 2019). In contrast, prokaryotes lack such sophisticated compartmentalization systems. When a single prokaryotic strain is used to integrate complex metabolic pathways, it often encounters challenges such as high metabolic burden, low efficiency, and poor genetic stability (Akdemir et al., 2022; Thuan et al., 2022). To address these issues, here we developed an obligate mutualistic prokaryotic co-culture system for the production of complex natural products, specifically flavonoids and their glycosides. This symbiotic system mimics eukaryotic compartmental synthesis by distributing different modules of the artificial biosynthetic pathways of flavonoids and glycosides established in this study among various bacterial members. This approach effectively reduced the metabolic burden, stabilized the metabolic flux through carbon source orthogonality, improved the overall efficiency, and achieved efficient synthesis of target products. Utilizing a plug-and-play modular design, enzyme screening, and fine-tuning of expression levels, we achieved the *de novo* synthesis of a series of flavonoids and mono-glycosides, including the first microbial heterologous synthesis of diosmetin, apigenin-Glu, luteolin-Glu, acacetin-Glu, isosakuranetin-Glu, hesperetin-Glu, and diosmetin-Glu.

Flavonoid glycosides consist of two parts: the flavonoid aglycone core and the glycosyl group. Due to the structural similarity of the aglycones, downstream glycosyltransferases often exhibit broad substrate promiscuity, leading to the formation of by-products. In this study, we demonstrated that this issue could be significantly mitigated through metabolic division engineering in microbial co-culture systems. This was

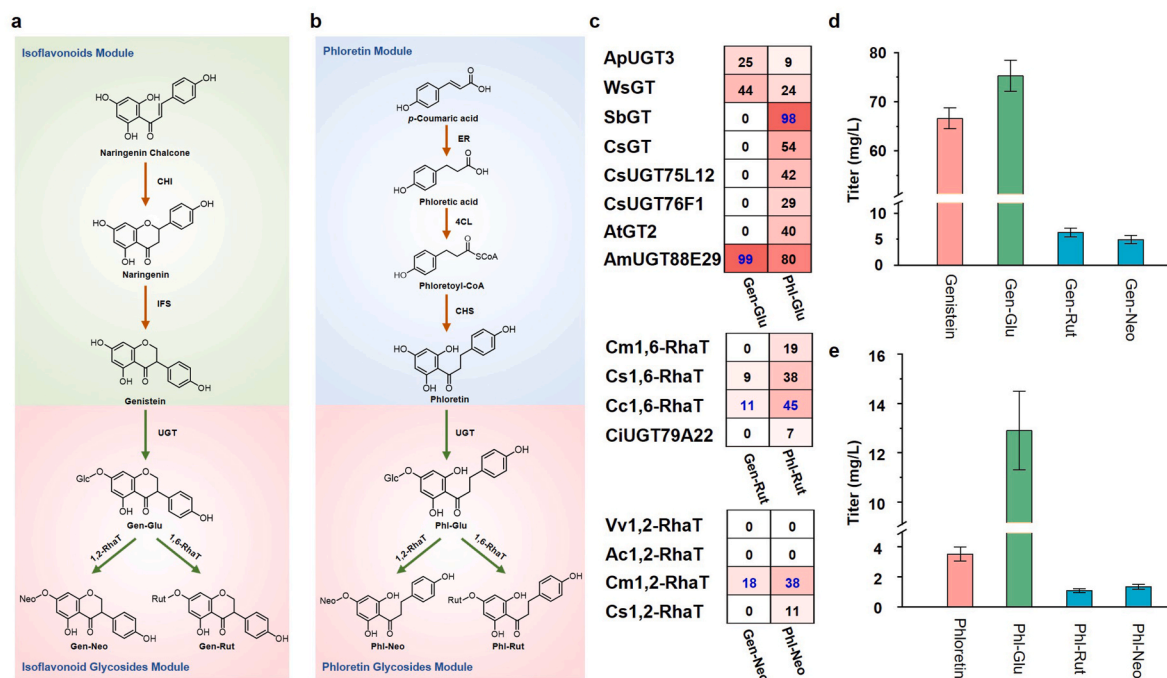


Fig. 8. Biosynthesis of isoflavonoid and dihydrochalcone glycosides. (a) The biosynthetic pathway of the isoflavonoid genistein and glycosides. (b) The biosynthetic pathway of the dihydrochalcone phloretin and glycosides. (c) Screening of UGTs and RhaTs for glycosylation of genistein and phloretin. The numbers represent the conversion rate (%). (d) The yields of genistein and glycosides. (e) The yields of phloretin and glycosides. Data shown are mean \pm SD ($n = 3$ independent experiments). Phl: phloretin; Gen: genistein; IFS: isoflavonoid synthase; ER: enoate reductase.

achieved by strategically selecting metabolic splitting nodes and allocating metabolic modules to different strains within the co-culture system. Flavonoid UGTs can glycosylate naringenin instead of naringenin-chalcone. By selecting naringenin chalcone (instead of naringenin) as the splitting node and distributing the flavonoid synthesis module and glycoside synthesis module into two *E. coli* strains, we successfully developed a three-bacteria co-culture system that efficiently produced the target flavonoid glycosides with minimal accumulation of naringenin-Glu. This approach was validated by successful production of diosmin (diosmetin-Rut) and neodiosmin (diosmetin-Neo), which are the flavonoid glycosides with the longest biosynthetic pathways studied here, synthesized by a total of 12 heterologous enzymes starting from tyrosine. To our knowledge, this study is the first report of *de novo* production of various flavonoid-di-glycosides.

By substituting the flavonoid skeleton synthesis module and the flavonoid synthesis module, our microbial co-culture systems achieved the *de novo* synthesis of the isoflavonoid, the dihydrochalcone and their glycosides. We anticipate that this approach of metabolic division engineering in microbial co-cultures could be extended to other products with long biosynthetic pathways, such as terpenoids and alkaloids.

CRedit authorship contribution statement

Zetian Qiu: Writing – original draft, Methodology, Formal analysis, Data curation. **Yumei Han:** Methodology, Data curation. **Jia Li:** Methodology, Investigation, Conceptualization. **Yi Ren:** Methodology, Data curation. **Xue Liu:** Methodology, Formal analysis. **Shengying Li:** Writing – review & editing, Supervision, Funding acquisition, Conceptualization. **Guang-Rong Zhao:** Writing – review & editing, Validation, Supervision, Methodology, Funding acquisition, Conceptualization. **Lei Du:** Writing – review & editing, Validation, Supervision, Methodology, Funding acquisition, Conceptualization.

Declaration of competing interest

The authors declare no competing financial interest.

Acknowledgments

This work was supported by the National Key Research and Development Program of China (2021YFA0911500), the Key-Area Research and Development Program of Guangdong Province (2020B0303070002), the National Natural Science Foundation of China (32370032, 32170088), the Shandong Provincial Natural Science Foundation (ZR2020ZD23), and the Taishan Young Scholars (tsqn202312032).

Appendix A. Supplementary data

Supplementary data to this article can be found online at <https://doi.org/10.1016/j.ymben.2025.02.001>.

Data availability

Data will be made available on request.

References

- Akdemir, H., Liu, Y., Zhuang, L., Zhang, H., Koffas, M.A., 2022. Utilization of microbial cocultures for converting mixed substrates to valuable bioproducts. *Curr. Opin. Microbiol.* 68, 102157. <https://doi.org/10.1016/j.mib.2022.102157>.
- Ali, F., Rahul, Naz, F., Jyoti, S., Siddique, Y.H., 2017. Health functionality of apigenin: a review. *Int. J. Food Prop.* 20 (6), 1197–1238. <https://doi.org/10.1080/10942912.2016.1207188>.
- Aulakh, S.K., Vidal, L.S., South, E.J., Peng, H.D., Varma, S.J., Herrera-Dominguez, L., Ralsler, M., Ledesma-Amaro, R., 2023. Spontaneously established syntrophic yeast communities improve bioproduction. *Nat. Chem. Biol.* 19 (8), 951–961. <https://doi.org/10.1038/s41589-023-01341-2>.
- Bennett, A.A., Mahood, E.H., Fan, K., Moghe, G.D., 2021. Untargeted metabolomics of purple and orange-fleshed sweet potatoes reveals a large structural diversity of anthocyanins and flavonoids. *Sci. Rep.* 11 (1), 16408. <https://doi.org/10.1038/s41598-021-95901-y>.

- Brooks, S.M., Marsan, C., Reed, K.B., Yuan, S.F., Nguyen, D.D., Trivedi, A., Altin-Yavuzarslan, G., Ballinger, N., Nelson, A., Alper, H.S., 2023. A tripartite microbial co-culture system for de novo biosynthesis of diverse plant phenylpropanoids. *Nat. Commun.* 14 (1), 4448. <https://doi.org/10.1038/s41467-023-40242-9>.
- Cabulong, R.B., Banares, A.B., Nisola, G.M., Lee, W.K., Chung, W.J., 2021. Applied and environmental microbiology metabolically engineered *Escherichia coli*. *Bioproc. Biosyst. Eng.* 44 (6), 1081–1091. <https://doi.org/10.1007/s00449-020-02502-6>.
- Chaves, J.O., de Souza, M.C., da Silva, L.C., Lachos-Perez, D., Torres-Mayanga, P.C., Machado, A.P.D., Forster-Carneiro, T., Vázquez-Espinosa, M., González-de-Peredo, A.V., Barbero, G.F., Rostagno, M.A., 2020. Extraction of flavonoids from natural sources using modern techniques. *Front. Chem.* 8, 507887. <https://doi.org/10.3389/fchem.2020.507887>.
- Cheah, L., Liu, L., Plan, M.R., Peng, B.Y., Lu, Z.Y., Schenk, G., Vickers, C.E., Sainsbury, F., 2023. Product profiles of promiscuous enzymes can be altered by controlling in vivo spatial organization. *Adv. Sci.* 10 (32), 2303415. <https://doi.org/10.1002/adv.202303415>.
- Chen, M.L., Ma, C.W., Lin, C., Zeng, A.P., 2021. Integrated laboratory evolution and rational engineering of GalP/Glk-dependent *Escherichia coli* for higher yield and productivity of L-tryptophan biosynthesis. *Metab. Eng. Commun.* 12, e00167. <https://doi.org/10.1016/j.mec.2021.e00167>.
- Chen, W., Yao, J., Meng, J., Han, W.J., Tao, Y., Chen, Y.H., Guo, Y.X., Shi, G.Z., He, Y., Jin, J.M., Tang, S.Y., 2019. Promiscuous enzymatic activity-aided multiple-pathway network design for metabolic flux rearrangement in hydroxytyrosol biosynthesis. *Nat. Commun.* 10, 960. <https://doi.org/10.1038/s41467-019-08781-2>.
- Deepika, Maurya, P.K., 2022. Health benefits of quercetin in age-related diseases. *Molecules* 27 (8), 2498. <https://doi.org/10.3390/molecules27082498>.
- Deng, Z.R., Hassan, S., Rafiq, M., Li, H.S., He, Y., Cai, Y., Kang, X., Liu, Z.G., Yan, T.D., 2020. Pharmacological activity of eriodictyol: the major natural polyphenolic flavanone. *Evid. Based Complementary Altern. Med.* 11. <https://doi.org/10.1155/2020/6681352>, 2020.
- Du, L., Li, S., 2021. Compartmentalized biosynthesis of fungal natural products. *Curr. Opin. Biotechnol.* 69, 128–135. <https://doi.org/10.1016/j.copbio.2020.12.006>.
- Duan, Y.Y., Du, W.Y., Song, Z.J., Chen, R.D., Xie, K.B., Liu, J.M., Chen, D.W., Dai, J.G., 2023. Functional characterization of a cycloartenol synthase and four glycosyltransferases in the biosynthesis of cycloastragenol-type astragalosides from *Astragalus membranaceus*. *Acta Pharm. Sin. B* 13 (1), 271–283. <https://doi.org/10.1016/j.apsb.2022.05.015>.
- Eichenberger, M., Lehka, B.J., Folly, C., Fischer, D., Martens, S., Simon, E., Naesby, M., 2017. Metabolic engineering of *Saccharomyces cerevisiae* for de novo production of dihydrochalcones with known antioxidant, antidiabetic, and sweet tasting properties. *Metab. Eng.* 39, 80–89. <https://doi.org/10.1016/j.ymben.2016.10.019>.
- Falcone Ferreyra, M.L., Rius, S.P., Casati, P., 2012. Flavonoids: biosynthesis, biological functions, and biotechnological applications. *Front. Plant Sci.* 3, 222. <https://doi.org/10.3389/fpls.2012.00222>.
- Fang, L.X., Fan, J., Luo, S.L., Chen, Y.R., Wang, C.Y., Cao, Y.X., Song, H., 2021. Genome-scale target identification in *Escherichia coli* for high-titer production of free fatty acids. *Nat. Commun.* 12 (1), 4976. <https://doi.org/10.1038/s41467-021-25243-w>.
- Feng, Y., Yao, M., Wang, Y., Ding, M., Zha, J., Xiao, W., Yuan, Y., 2020. Advances in engineering UDP-sugar supply for recombinant biosynthesis of glycosides in microbes. *Biotechnol. Adv.* 41, 107538. <https://doi.org/10.1016/j.biotechadv.2020.107538>.
- Fujiwara, R., Noda, S., Tanaka, T., Kondo, A., 2020. Metabolic engineering of *Escherichia coli* for shikimate pathway derivative production from glucose-xylose co-substrate. *Nat. Commun.* 11 (1), 279. <https://doi.org/10.1038/s41467-020-14710-5>.
- Gerges, S.H., Wahdan, S.A., Elsherbiny, D.A., El-Demerdash, E., 2022. Pharmacology of diosmin, a citrus flavone glycoside: an updated review. *Eur. J. Drug Metab. Pharmacokinet.* 47 (1), 1–18. <https://doi.org/10.1007/s13318-021-00731-y>.
- Guo, F., Zhang, X.W., You, C., Zhang, C.J., Li, F.W., Li, N., Xia, Y.W., Liu, M.Y., Qiu, Z.T., Zheng, X.L., Ma, L., Zhang, G., Luo, L.Z., Cao, F., Feng, Y.G., Zhao, G.R., Zhang, W., Li, S.Y., Du, L., 2022. Diversification of phenolic glycosides by two UDP-glycosyltransferases featuring complementary regioselectivity. *Microb. Cell Fact.* 21 (1), 208. <https://doi.org/10.1186/s12934-022-01935-w>.
- Hofer, B., 2016. Recent developments in the enzymatic O-glycosylation of flavonoids. *Appl. Microbiol. Biotechnol.* 100 (10), 4269–4281. <https://doi.org/10.1007/s00253-016-7465-0>.
- Huang, F.C., Hinkelmann, J., Hermenau, A., Schwab, W., 2016. Enhanced production of β -glucosides by in-situ UDP-glucose regeneration. *J. Biotechnol.* 224, 35–44. <https://doi.org/10.1016/j.jbiotec.2016.02.022>.
- Janyou, A., Moohammadare, A., Jumnonprakhon, P., Tocharus, C., Chokchaisiri, R., Suksamrarn, A., Tocharus, J., 2023. Effects of isosakuranetin on cerebral infarction and blood brain barrier damage from cerebral ischemia/reperfusion injury in a rat model. *J. Biomol. Struct. Dyn.* 42 (2), 1064–1071. <https://doi.org/10.1080/07391102.2023.2205940>.
- Ji, Y., Li, B.Z., Qiao, M., Li, J.M., Xu, H., Zhang, L.H., Zhang, X., 2020. Advances on the in vivo and in vitro glycosylations of flavonoids. *Appl. Microbiol. Biotechnol.* 104 (15), 6587–6600. <https://doi.org/10.1007/s00253-020-10667-z>.
- Jiang, N., Dillon, F.M., Silva, A., Gomez-Cano, L., Grotewold, E., 2021. Rhamnose in plants - from biosynthesis to diverse functions. *Plant Sci.* 302, 110687. <https://doi.org/10.1016/j.plantsci.2021.110897>.
- Jucá, M.M., Cysne, F.M.S., de Almeida, J.C., Mesquita, D.D., Barriga, J.R.D., Ferreira, K.C.D., Barbosa, T.M., Vasconcelos, L.C., Leal, L.K.A.M., Honorio, J.E.R., Vasconcelos, S.M.M., 2020. Flavonoids: biological activities and therapeutic potential. *Nat. Prod. Res.* 34 (5), 692–705. <https://doi.org/10.1080/14786419.2018.1493588>.
- Kiriya, Y., Tokumaru, H., Sadamoto, H., Kobayashi, S., Nochi, H., 2024. Effects of phenolic acids produced from food-derived flavonoids and amino acids by the gut microbiota on health and disease. *Molecules* 29 (21), 5102. <https://doi.org/10.3390/molecules29215102>.
- Klena, J.D., Schnaitman, C.A., 1993. Function of the *rfb* gene cluster and the *rfe* gene in the synthesis of O antigen by *Shigella dysenteriae* 1. *Mol. Microbiol.* 9 (2), 393–402. <https://doi.org/10.1111/j.1365-2958.1993.tb01700.x>.
- Koma, D., Kishida, T., Yoshida, E., Ohashi, H., Yamanaka, H., Moriyoshi, K., Nagamori, E., Ohmoto, T., 2020. Chromosome engineering to generate plasmid-free phenylalanine- and tyrosine-overproducing *Escherichia coli* strains that can be applied in the generation of aromatic-compound-producing bacteria. *Appl. Environ. Microbiol.* 86 (14), e00525. <https://doi.org/10.1128/AEM.00525-20>.
- Lan, H.N., Liu, R.Y., Liu, Z.H., Li, X., Li, B.Z., Yuan, Y.J., 2023. Biological valorization of lignin to flavonoids. *Biotechnol. Adv.* 64, 108107. <https://doi.org/10.1016/j.biotechadv.2023.108107>.
- Li, H.L., Wei, Y.Y., Li, X.H., Zhang, S.S., Zhang, R.T., Li, J.H., Ma, B.W., Shao, S.B., Lv, Z.W., Ruan, H., Zhou, H.G., Yang, C., 2022a. Diosmetin has therapeutic efficacy in colitis regulating gut microbiota, inflammation, and oxidative stress via the circ-Sirt1/Sirt1 axis. *Acta Pharmacol. Sin.* 43 (4), 919–932. <https://doi.org/10.1038/s41401-021-00726-0>.
- Li, J., Qiu, Z.T., Zhao, G.R., 2022b. Modular engineering of *E. coli* coculture for efficient production of resveratrol from glucose and arabinose mixture. *Synth. Syst. Biotechnol.* 7 (2), 718–729. <https://doi.org/10.1016/j.synbio.2022.03.001>.
- Li, X.L., Zhou, Z., Li, W.N., Yan, Y.J., Shen, X.L., Wang, J., Sun, X.X., Yuan, Q.P., 2022c. Design of stable and self-regulated microbial consortia for chemical synthesis. *Nat. Commun.* 13 (1), 1554. <https://doi.org/10.1038/s41467-022-29215-6>.
- Liu, J.C., De La Pena, R., Tocol, C., Sattely, E.S., 2024. Reconstitution of early paclitaxel biosynthetic network. *Nat. Commun.* 15 (1), 1419. <https://doi.org/10.1038/s41467-024-45574-8>.
- Liu, Q., Yu, T., Li, X., Chen, Y., Campbell, K., Nielsen, J., Chen, Y., 2019. Rewiring carbon metabolism in yeast for high level production of aromatic chemicals. *Nat. Commun.* 10 (1), 4976. <https://doi.org/10.1038/s41467-019-12961-5>.
- Liu, X., Li, L.L., Zhao, G.R., 2022a. Systems metabolic engineering of *Escherichia coli* coculture for de novo production of genistein. *ACS Synth. Biol.* 11 (5), 1746–1757. <https://doi.org/10.1021/acssynbio.1c00590>.
- Liu, X., Li, X.B., Jiang, J.L., Liu, Z.N., Qiao, B., Li, F.F., Cheng, J.S., Sun, X.C., Yuan, Y.J., Qiao, J.J., Zhao, G.R., 2018. Convergent engineering of syntrophic *Escherichia coli* coculture for efficient production of glycosides. *Metab. Eng.* 47, 243–253. <https://doi.org/10.1016/j.ymben.2018.03.016>.
- Liu, X., Liu, J.C., Lei, D.W., Zhao, G.R., 2022b. Modular metabolic engineering for production of phloretic acid, phloretin and phlorizin in *Escherichia coli*. *Chem. Eng. Sci.* 247, 116931. <https://doi.org/10.1016/j.ces.2021.116931>.
- Liu, Y.Y., Li, X.N., Sui, S.Y., Tang, J.S., Chen, D.W., Kang, Y.Y., Xie, K.B., Liu, J.M., Lan, J.Q., Wu, L., Chen, R.D., Peng, Y., Dai, J.G., 2023. Structural diversification of bioactive bibenzyls through modular co-culture leading to the discovery of a novel neuroprotective agent. *Acta Pharm. Sin. B* 13 (4), 1771–1785. <https://doi.org/10.1016/j.apsb.2022.10.007>.
- Louie, T.M., Xie, X.S., Xun, L.Y., 2003. Coordinated production and utilization of FADH₂ by NAD(P)H-flavin oxidoreductase and 4-hydroxyphenylacetate 3-monooxygenase. *Biochemistry* 42 (24), 7509–7517. <https://doi.org/10.1021/bi034092r>.
- Lv, Y.K., Marsafari, M., Koffas, M., Zhou, J.W., Xu, P., 2019. Optimizing oleaginous yeast cell factories for flavonoids and hydroxylated flavonoids biosynthesis. *ACS Synth. Biol.* 8 (11), 2514–2523. <https://doi.org/10.1021/acssynbio.9b00193>.
- Mao, Z.C., Shin, H.D., Chen, R.R.Z., 2006. Engineering the *E. coli* UDP-glucose synthesis pathway for oligosaccharide synthesis. *Biotechnol. Prog.* 22 (2), 369–374. <https://doi.org/10.1021/bp0503181>.
- Martens, S., Forkmann, G., Matern, U., Lukacin, R., 2001. Cloning of parsley flavone synthase I. *Phytochemistry* 58 (1), 43–46. [https://doi.org/10.1016/S0031-9422\(01\)00191-1](https://doi.org/10.1016/S0031-9422(01)00191-1).
- Martens, S., Mithöfer, A., 2005. Flavones and flavone synthases. *Phytochemistry* 66 (20), 2399–2407. <https://doi.org/10.1016/j.phytochem.2005.07.013>.
- Maruyama, H., Sumitou, Y., Sakamoto, T., Apaki, Y., Hara, H., 2009. Antihypertensive effects of flavonoids isolated from Brazilian green propolis in spontaneously hypertensive rats. *Biol. Pharm. Bull.* 32 (7), 1244–1250. <https://doi.org/10.1248/bpb.32.1244>.
- Ohashi, T., Hasegawa, Y., Masaki, R., Fujiyama, K., 2016. Substrate preference of citrus naringenin rhamnosyltransferases and their application to flavonoid glycoside production in fission yeast. *Appl. Microbiol. Biotechnol.* 100 (2), 687–696. <https://doi.org/10.1007/s00253-015-6982-6>.
- Pan, R.Z., Yang, X.Y., Qiu, M., Jiang, W.K., Zhang, W.M., Jiang, Y.J., Xin, F.X., Jiang, M., 2023. Construction of coculture system containing *Escherichia coli* with different microbial species for biochemical production. *ACS Synth. Biol.* 12 (8), 2208–2216. <https://doi.org/10.1021/acssynbio.3c00329>.
- Peng, L.F., Arauzo-Bravo, M.J., Shimizu, K., 2004. Metabolic flux analysis for a *ppc* mutant *Escherichia coli* based on ¹³C-labelling experiments together with enzyme activity assays and intracellular metabolite measurements. *FEMS Microbiol. Lett.* 235 (1), 17–23. <https://doi.org/10.1016/j.femsle.2004.04.003>.
- Peters, A., Schneiderpoetsch, H.A.W., Schwarz, H., Weissenböck, G., 1988. Biochemical and immunological characterization of chalcone synthase from rye leaves. *J. Plant Physiol.* 133 (2), 178–182. [https://doi.org/10.1016/S0176-1617\(88\)80134-2](https://doi.org/10.1016/S0176-1617(88)80134-2).
- Prasher, P., Sharma, M., Singh, S.K., Gulati, M., Chellappan, D.K., Zaccani, F., De Rubis, G., Gupta, G., Sharifi-Rad, J., Cho, W.C., Dua, K., 2022. Luteolin: a flavonoid with a multifaceted anticancer potential. *Cancer Cell Int.* 22 (1), 386. <https://doi.org/10.1186/s12935-022-02808-3>.
- Qiu, Z.T., Liu, X., Li, J., Qiao, B., Zhao, G.R., 2022. Metabolic division in an *Escherichia coli* coculture system for efficient production of kaempferide. *ACS Synth. Biol.* 11 (3), 1213–1227. <https://doi.org/10.1021/acssynbio.1c00510>.

- Ren, J., Lu, Y.F., Qian, Y.H., Chen, B.Z., Wu, T., Ji, G., 2019. Recent progress regarding kaempferol for the treatment of various diseases. *Exp. Ther. Med.* 18 (4), 2759–2776. <https://doi.org/10.3892/etm.2019.7886>.
- Ruprecht, C., Bönisch, F., Ilmberger, N., Heyer, T.V., Haupt, E.T.K., Streit, W.R., Rabausch, U., 2019. High level production of flavonoid rhamnosides by metagenome-derived glycosyltransferase C in *Escherichia coli* utilizing dextrans of starch as a single carbon source. *Metab. Eng.* 55, 212–219. <https://doi.org/10.1016/j.ymben.2019.07.002>.
- Saito, S., Tanaka, M., Satoh-Asahara, N., Carare, R.O., Ihara, M., 2021. Taxifolin: a potential therapeutic agent for cerebral amyloid angiopathy. *Front. Pharmacol.* 12, 643357. <https://doi.org/10.3389/fphar.2021.643357>.
- Santos, C.N.S., Koffas, M., Stephanopoulos, G., 2011. Optimization of a heterologous pathway for the production of flavonoids from glucose. *Metab. Eng.* 13 (4), 397–400. <https://doi.org/10.1016/j.ymben.2011.02.002>.
- Schenck, C.A., Holland, C.K., Schneider, M.R., Men, Y., Lee, S.G., Jez, J.M., Maeda, H.A., 2017. Molecular basis of the evolution of alternative tyrosine biosynthetic routes in plants. *Nat. Chem. Biol.* 13 (9), 1029–1035. <https://doi.org/10.1038/Nchembio.2414>.
- Sekar, B.S., Lukito, B.R., Li, Z., 2019. Production of natural 2-phenylethanol from glucose or glycerol with coupled *Escherichia coli* strains expressing L-phenylalanine biosynthesis pathway and artificial biocascades. *ACS Sustain. Chem. Eng.* 7 (14), 12231–12239. <https://doi.org/10.1021/acssuschemeng.9b01569>.
- Singh, S., Gupta, P., Meena, A., Luqman, S., 2020. Acacetin, a flavone with diverse therapeutic potential in cancer, inflammation, infections and other metabolic disorders. *Food Chem. Toxicol.* 145, 111708. <https://doi.org/10.1016/j.fct.2020.111708>.
- Soma, Y., Tsuruno, K., Wada, M., Yokota, A., Hanai, T., 2014. Metabolic flux redirection from a central metabolic pathway toward a synthetic pathway using a metabolic toggle switch. *Metab. Eng.* 23, 175–184. <https://doi.org/10.1016/j.ymben.2014.02.008>.
- Sun, J., Sun, W., Zhang, G., Lv, B., Li, C., 2022. High efficient production of plant flavonoids by microbial cell factories: challenges and opportunities. *Metab. Eng.* 70, 143–154. <https://doi.org/10.1016/j.ymben.2022.01.011>.
- Takamura, Y., Nomura, G., 1988. Changes in the intracellular concentration of acetyl-CoA and malonyl-CoA in relation to the carbon and energy metabolism of *Escherichia coli* K12. *J. Gen. Microbiol.* 134, 2249–2253. <https://doi.org/10.1099/00221287-134-8-2249>.
- Tang, D.D., Zheng, X.L., Zhao, Y.S., Zhang, C.S., Chen, C., Chen, Y.X., Du, L., Liu, K., Li, S.Y., 2024. Engineered microbial consortium for *de novo* production of sclareolide. *J. Agric. Food Chem.* 72 (36), 19977–19984. <https://doi.org/10.1021/acs.jafc.4c05506>.
- Thuan, N.H., Tatipamula, V.B., Canh, N.X., Van Giang, N., 2022. Recent advances in microbial co-culture for production of value-added compounds. *3 Biotech.* 12 (5), 115. <https://doi.org/10.1007/s13205-022-03177-4>.
- Tuli, H.S., Rath, P., Chauhan, A., Sak, K., Aggarwal, D., Choudhary, R., Sharma, U., Vashishth, K., Sharma, S., Kumar, M., Yadav, V., Singh, T., Yerer, M.B., Haque, S., 2022. Luteolin, a potent anticancer compound: from chemistry to cellular interactions and synergetic perspectives. *Cancers* 14 (21), 5373. <https://doi.org/10.3390/cancers14215373>.
- Waki, T., Takahashi, S., Nakayama, T., 2021. Managing enzyme promiscuity in plant specialized metabolism: a lesson from flavonoid biosynthesis. *Bioessays* 43 (3), 2000164. <https://doi.org/10.1002/bies.202000164>.
- Wang, H.Y., Wang, S.Y., Wang, J., Shen, X.L., Feng, X.D., Yuan, S.G., Sun, X.X., Yuan, Q.P., 2022a. Engineering a prokaryotic non-P450 hydroxylase for 3'-hydroxylation of flavonoids. *ACS Synth. Biol.* 11 (11), 3865–3873. <https://doi.org/10.1021/acssynbio.2c00430>.
- Wang, L., Wang, H.J., Chen, J.B., Qin, Z.J., Yu, S.Q., Zhou, J.W., 2023a. Coordinating caffeic acid and salvanic acid A pathways for efficient production of rosmarinic acid in *Escherichia coli*. *Metab. Eng.* 76, 29–38. <https://doi.org/10.1016/j.ymben.2023.01.002>.
- Wang, R., Su, Y., Yang, W., Zhang, H., Wang, J., Gao, W., 2024a. Enhanced precision and efficiency in metabolic regulation: compartmentalized metabolic engineering. *Bioresour. Technol.* 402, 130786. <https://doi.org/10.1016/j.biortech.2024.130786>.
- Wang, Z., Li, X., Dai, Y., Yin, L., Azi, F., Zhou, J., Dong, M., Xia, X., 2022b. Sustainable production of genistin from glycerol by constructing and optimizing *Escherichia coli*. *Metab. Eng.* 74, 206–219. <https://doi.org/10.1016/j.ymben.2022.10.015>.
- Wang, Z.L., Du, X.Q., Ye, G., Wang, H.T., Liu, Y.Z., Liu, C.R., Li, F.D., Ágren, H., Zhou, Y., Li, J.H., He, C., Guo, D.A., Ye, M., 2024b. Functional characterization, structural basis, and protein engineering of a rare flavonoid 2'-O-glycosyltransferase from *Scutellaria baicalensis*. *Acta Pharm. Sin. B* 14 (8), 3746–3759. <https://doi.org/10.1016/j.apsb.2024.04.001>.
- Wang, Z.X., Zhou, Y., Wang, Y.F., Yan, X.H., 2023b. Reconstitution and optimization of the maresin biosynthetic pathway in yeast. *ACS Synth. Biol.* 12 (10), 2922–2933. <https://doi.org/10.1021/acssynbio.3c00267>.
- Whitehead, I.M., Dixon, R.A., 1983. Chalcone synthase from cell suspension cultures of *Phaseolus vulgaris* L. *Biochim. Biophys. Acta* 747 (3), 298–303. [https://doi.org/10.1016/0167-4838\(83\)90109-7](https://doi.org/10.1016/0167-4838(83)90109-7).
- Xiao, Z.Q., Wang, Y.T., Liu, J., Zhang, S.Q., Tan, X.J., Zhao, Y.F., Mao, J.W., Jiang, N., Zhou, J.W., Shan, Y., 2023. Systematic engineering of *Saccharomyces cerevisiae* chassis for efficient flavonoid-7-O-disaccharide biosynthesis. *ACS Synth. Biol.* 12 (9), 2740–2749. <https://doi.org/10.1021/acssynbio.3c00348>.
- Xiong, Y.J., Chu, H.W., Lin, Y., Han, F., Li, Y.C., Wang, A.G., Wang, F.J., Chen, D.P., Wang, J.Y., 2016. Hesperidin alleviates rat postoperative ileus through anti-inflammation and stimulation of Ca²⁺-dependent myosin phosphorylation. *Acta Pharmacol. Sin.* 37 (8), 1091–1100. <https://doi.org/10.1038/aps.2016.56>.
- Xu, Y., Wang, X., Zhang, C., Zhou, X., Xu, X., Han, L., Lv, X., Liu, Y., Liu, S., Li, J., Du, G., Chen, J., Ledesma-Amaro, R., Liu, L., 2022. De novo biosynthesis of rubusoside and rebaudioside in engineered yeasts. *Nat. Commun.* 13 (1), 3040. <https://doi.org/10.1038/s41467-022-30826-2>.
- Xun, L.Y., Sandvik, E.R., 2000. Characterization of 4-hydroxyphenylacetate 3-hydroxylase (HpaB) of *Escherichia coli* as a reduced flavin adenine dinucleotide-utilizing monooxygenase. *Appl. Environ. Microbiol.* 66 (2), 481–486. <https://doi.org/10.1128/Aem.66.2.481-486.2000>.
- Yan, D., Kim, W.J., Yoo, S.M., Choi, J.H., Ha, S.H., Lee, M.H., Lee, S.Y., 2018. Repurposing type III polyketide synthase as a malonyl-CoA biosensor for metabolic engineering in bacteria. *Proc. Natl. Acad. Sci. U.S.A.* 115 (40), 9835–9844. <https://doi.org/10.1073/pnas.1808567115>.
- Yan, R., Xie, B., Xie, K., Liu, Q., Sui, S., Wang, S., Chen, D., Liu, J., Chen, R., Dai, J., Yang, L., 2024. Unravelling and reconstructing the biosynthetic pathway of bergenin. *Nat. Commun.* 15 (1), 3539. <https://doi.org/10.1038/s41467-024-47502-2>.
- Yang, S., Chen, R.B., Cao, X., Wang, G.D., Zhou, Y.J., 2024. De novo biosynthesis of the hops bioactive flavonoid xanthohumol in yeast. *Nat. Commun.* 15 (1), 253. <https://doi.org/10.1038/s41467-023-44654-5>.
- Yao, Y.F., Wang, C.S., Qiao, J., Zhao, G.R., 2013. Metabolic engineering of *Escherichia coli* for production of salvanic acid A via an artificial biosynthetic pathway. *Metab. Eng.* 19, 79–87. <https://doi.org/10.1016/j.ymben.2013.06.001>.
- Yeh, C.H., Shen, Z.Q., Wang, T.W., Kao, C.H., Teng, Y.C., Yeh, T.K., Lu, C.K., Tsai, T.F., 2022. Hesperetin promotes longevity and delays aging via activation of *cisd2* in naturally aged mice. *J. Biomed. Sci.* 29 (1), 53. <https://doi.org/10.1186/s12929-022-00838-7>.
- Zhang, J.Q., Hu, C., Li, X.L., Liang, L., Zhang, M.C., Chen, B., Liu, X.H., Yang, D.C., 2021. Protective effect of dihydrokaempferol on acetaminophen-induced liver injury by activating the SIRT1 pathway. *Am. J. Chin. Med.* 49 (3), 705–718. <https://doi.org/10.1142/S0192415x21500324>.
- Zhang, W., Du, L., Qu, Z.P., Zhang, X.W., Li, F.W., Li, Z., Qi, F.F., Wang, X., Jiang, Y.Y., Men, P., Sun, J.R., Cao, S.N., Geng, C., Qi, F.X., Wan, X.B., Liu, C.N., Li, S.Y., 2019. Compartmentalized biosynthesis of mycophenolic acid. *Proc. Natl. Acad. Sci. U.S.A.* 116 (27), 13305–13310. <https://doi.org/10.1073/pnas.1821932116>.
- Zhao, Y., Wu, B.H., Liu, Z.N., Qiao, J.J., Zhao, G.R., 2018. Combinatorial optimization of resveratrol production in engineered *E. coli*. *J. Agric. Food Chem.* 66 (51), 13444–13453. <https://doi.org/10.1021/acs.jafc.8b05014>.
- Zheng, J., Zhao, C.N., Liao, Z.K., Liu, X.J., Gong, Q., Zhou, C.W., Liu, Y.L., Wang, Y., Cao, J.P., Liu, L.L., Wang, D.L., Sun, C.G., 2023. Functional characterization of two flavone synthase II members in citrus. *Hortic. Res.* 10 (7), 113. <https://doi.org/10.1093/hr/uhad113>.